Infrared Spectra and Density Functional Calculations of $RuCO^+$, $OsCO^+$, $Ru(CO)_x$, $Os(CO)_x$, $Ru(CO)_x^-$ and $Os(CO)_x^-$ ($x = 1-4$) in Solid Neon

Mingfei Zhou and Lester Andrews*

Department of Chemistry, University of Virginia, Charlottesville, Virginia 22901

Received: March 10, 1999; In Final Form: May 27, 1999

Laser-ablated ruthenium and osmium atoms, cations and electrons have been reacted with CO molecules during condensation in excess neon. The $Ru(CO)_x$ and $Os(CO)_x$ ($x = 1-5$) molecules are formed during sample deposition or on annealing. The $Ru(CO)_x^-$ and $Os(CO)_x^-$ ($x = 1-4$) anions are formed by electron capture, and the $RuCO^+$ and $OsCO^+$ cations are produced by metal cation reactions and identified from ^{13}CO and $C^{18}O$ isotopic substitution, density functional calculations, and behavior on doping with CCl_4 to serve as an electron trap. Density functional calculations predict these frequencies within 1% and the isotopic shifts for different C−O stretching modes within averages of 1 to 2 cm^{-1} including vibrational modes for both C_{3v} and D_{2d} tetracarbonyl anion structures.

Introduction

Transition metal carbonyls are important in organometallic chemistry, and studies of these molecules have been the focus of extensive and continuous study.[1] Although unsaturated iron carbonyls have been well studied,[2−12] ruthenium and osmium carbonyls have received far less attention because the ruthenium and osmium pentacarbonyl precursor molecules are very unstable. Earlier infrared investigations suggest that $Ru(CO)_5$ and $Os(CO)_5$ have trigonal bipyramidal configurations with D_{3h} symmetry in the gas phase and in heptane solution,[13,14] and a later study of ^{13}CO-enriched $Ru(CO)_5$ in liquid xenon is also consistent with D_{3h} symmetry.[15] This structure has been confirmed by more recent electron diffraction studies in the gas phase[16,17] and by theoretical calculations.[18−22] The infrared spectrum of $Os(CO)_4$ has been observed from photolysis of $Os(CO)_5$ in a methane matrix,[23] and broad absorptions have been reported for the tricarbonyls and tetracarbonyls in gas-phase time-resolved infrared spectroscopic studies.[24,25] Finally, theoretical calculations for the tetracarbonyls predict C_{2v} symmetry analogous to $Fe(CO)_4$,[18−22] but there are no calculations for the Ru and Os mono-, di-, and tricarbonyls.

Recent pulsed-laser ablation matrix isolation studies in this laboratory have shown that laser ablation is an effective method to produce reactive metal atoms as well as cations and electrons, and as a result, metal carbonyls can be synthesized, molecular anions can be formed via electron capture by neutral molecules, and molecular cations can be produced by metal cation reactions.[12,26−28] In the iron system, $FeCO^+$ and $Fe(CO)_{1-4}^-$ anions and neutral iron carbonyls were produced and identified via isotopic substitution and density functional calculations.[12] The lack of experimental data on the lower ruthenium and osmium carbonyls prompted this investigation using laser-ablated ruthenium and osmium atoms, cations and electrons, and carbon monoxide.

Experimental Section

The experiment for laser ablation and matrix isolation spectroscopy has been described in detail previously.[12,29,30] In brief, the Nd:YAG laser fundamental (1064-nm, 10-Hz repetition rate, 10-ns pulse width) was focused on the rotating metal target using low energy (1−5 mJ/pulse). Laser-ablated metal atoms were co-deposited with carbon monoxide (0.05−0.2%) in excess neon onto a 4 K CsI cryogenic window at 2−4 mmol/h for 30−60 min. Carbon monoxide (Matheson) and isotopic $^{13}C^{16}O$ and $^{12}C^{18}O$ (Cambridge Isotopic Laboratories) and selected mixtures were used in different experiments. Fourier transform infrared (FTIR) spectra were recorded at 0.5 cm^{-1} resolution on a Nicolet 750 spectrometer with 0.1 cm^{-1} accuracy using a HgCdTe detector. Matrix samples were annealed at different temperatures, and selected samples were subjected to broadband photolysis by a medium-pressure mercury arc (Philips, 175 W, globe removed, 240−580 nm) and glass filters.

Results

Infrared spectra of Ru+CO and Os+CO systems will be presented followed by density functional calculations of potential metal carbonyl product species.

Ru+CO/Ne. Infrared spectra from laser-ablated Ru and 0.2% CO in neon are shown in Figures 1 and 2, and the absorptions are listed in Table 1A. Sample deposition reveals strong CO absorption at 2140.8 cm^{-1}, weak CO^+, $(CO)_2^+$ and $(CO)_2^-$ absorptions at 2194.3, 2056.3, and 1517.4 cm^{-1} (not shown).[31] In the 2080−1910 cm^{-1} region (Figure 1), strong bands at 1935.6 and 1955.3 cm^{-1}, and weak bands at 2049.8, 2023.5, 2012.3, 1983.0, 1975.4, 1970.6, and 1929.7 cm^{-1} are observed after deposition. Annealing to 6 and 8 K increased all these absorptions. Full-arc photolysis decreased the 1975.4, 1970.6, 1955.3, and 1935.6 cm^{-1} bands, and increased the 2049.8, 2023.5, and 2012.3 cm^{-1} absorptions, and a final annealing to 10 K increased all these absorptions. The weak band at 2134.9 cm^{-1} increased on annealing and disappeared on photolysis.

In the 1900−1750 cm^{-1} region (Figure 2), sample deposition produced 10 weak bands. Annealing to 6 and 8 K decreased the 1792.8 cm^{-1} band and slightly increased all other bands. Photolysis using the mercury arc and 470-nm long-wavelength pass filter had no obvious effect, but $\lambda > 380$ nm photolysis destroyed the 1792.8 cm^{-1} band and slightly increased the other absorptions.

* Electronic mail: lsa@virginia.edu.

10.1021/jp990846t CCC: $18.00 © 1999 American Chemical Society
Published on Web 08/12/1999

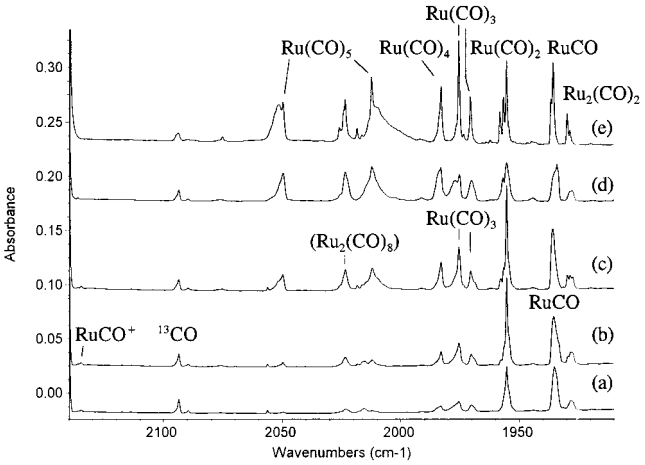

Figure 1. Infrared spectra in the 2140−1910 cm^{-1} region for laser-ablated Ru atoms co-deposited with 0.2% CO in neon: (a) after 30 min sample deposition at 4 K; (b) after annealing to 6 K; (c) after annealing to 8 K, (d) after 10 min full-arc photolysis; and (e) after annealing to 10 K.

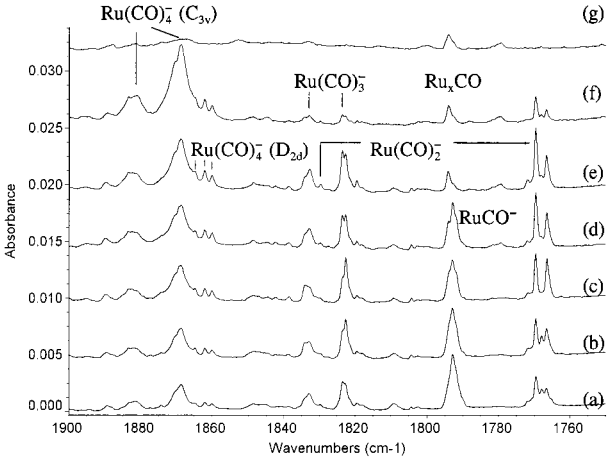

Figure 2. Infrared spectra in the 1900−1750 cm^{-1} region for laser-ablated Ru atoms co-deposited with 0.2% CO in neon: (a) after 30 min sample deposition at 4 K; (b) after annealing to 6 K; (c) after annealing to 8 K; (d) after 10 min $\lambda > 470$ nm photolysis; (e) after 10 min $\lambda > 380$ nm photolysis, (f) after 10 min $\lambda > 290$ nm photolysis; and (g) after 10 min full-arc photolysis.

Photolysis $\lambda > 290$ nm almost eliminated the 1766.5, 1769.6, 1822.7, and 1832.9 cm^{-1} bands, whereas the 1868.6 and 1881.0 cm^{-1} bands increased, but a final full-arc photolysis destroyed all these bands.

Experiments were also done using $^{13}C^{16}O$, $^{12}C^{18}O$, and mixed $^{12}C^{16}O+^{13}C^{16}O$ samples, and the isotopic frequencies are also listed in Table 1A. The spectra with mixed $^{12}C^{16}O+^{13}C^{16}O$ sample in the 2080−1880 and 1880−1720 cm^{-1} regions are shown in Figures 3 and 4, respectively.

Ru+CO/Ar. A set of experiments was done with 0.5, 0.2, 0.1, and 0.05% CO in argon, and the spectra appear much like the iron spectra in Figures 1 and 2 of ref 12. Figure 5 illustrates spectra for the 0.2% CO experiment. The stronger bands on deposition were at 1923.3 and 1917.7 cm^{-1} with weaker bands at 2039.1, 2003.8 cm^{-1} and at 1782.4, 1778.1, 1773.0 cm^{-1}. Annealing to 25 K increased the 1917.7 cm^{-1} band (5 ×) markedly increased the 2039.1, 2003.8 cm^{-1} bands (10 ×), and slightly decreased the lower set, but produced new weak 1882.0, 1862.4, 1834.2, 1810.3, and 1756.9 cm^{-1} absorptions. Broadband photolysis decreased the features below 1834.2 cm^{-1} and slightly increased the upper bands and weak absorptions in the 1960 cm^{-1} region. Annealing to 30 K increased the upper absorptions, but further annealing to 35 K decreased the 1917.7 cm^{-1} band and increased the 2039.1, 2003.8 cm^{-1} bands and blue satellite absorptions.

The $^{13}C^{16}O$ and $^{12}C^{18}O$ isotopic experiments and mixtures were done for Ru in argon, and the frequencies are listed in Table 1B.

Os+CO/Ne. Infrared spectra in the 2060−1960 and 1910−1770 cm^{-1} regions from laser-ablated Os and 0.2% CO in neon are shown in Figures 6 and 7, and the absorptions are listed in Table 2. In the upper region sample deposition reveals strong absorptions at 1966.2 and 1975.2 cm^{-1} with shoulders at 1973.8 and 1972.6 cm^{-1}. Annealing to 6 and 8 K decreased the 1972.6 cm^{-1} band, increased the 1966.2, 1973.8, and 1975.2 cm^{-1} bands, and produced new bands at 1983.1, 2003.2, and 2048.7 cm^{-1}. Broadband photolysis increased the 1972.6 cm^{-1} band, and further annealing to 10 and 12 K increased the 1966.2, 1973.8, 2003.2, and 2048.7 cm^{-1} bands. Eleven new product absorptions appeared in the lower region. Annealing to 8 K increased all of the product bands. Photolysis with $\lambda > 470$ and $\lambda > 380$ nm slightly increased the absorptions at the expense of the $(CO)_2^-$ absorption (not shown). A $\lambda > 290$ nm photolysis destroyed the 1785.5 cm^{-1} band, decreased the 1780.0, 1781.5, 1783.5, 1826.9, and 1843.1 cm^{-1} bands, and increased the broad 1862 and 1882.6 cm^{-1} bands and sharp 1858.3, 1860.4, and 1866.3 cm^{-1} bands. A final full-arc photolysis almost eliminated these absorptions.

Again, experiments were done using isotopic $^{13}C^{16}O$, $^{12}C^{18}O$, and mixed $^{12}C^{16}O+^{13}C^{16}O$ samples, and the results are also listed in Table 2. The spectra in the 2060−1910 and 1890−1730 cm^{-1} regions using the mixed $^{12}C^{16}O+^{13}C^{16}O$ sample are shown in Figures8 and 9.

CCl_4 Doping. Experiments were done with 0.02% CCl_4 added to serve as an electron trap for both Ru and Os + 0.1% CO systems. The absorptions assigned below to anions were almost eliminated from the spectra of the deposited samples, whereas the absorptions to be identified as cations were enhanced (3×) on doping with CCl_4, as found previously.[12]

Calculations. Density functional theory (DFT) calculations were done to support band identifications using the Gaussian 94 program.[32] The BP86 functional was used for most calculations, but comparisons also were done with the hybrid B3LYP functional.[33,34] The D95* basis sets for C and O atoms, and Los Alamos ECP plus DZ basis set for metal atoms with approximate treatment of relativistic effects were employed.[35,36] Calculations were first performed on the monocarbonyl neutrals, cations and anions using the BP86 functional, and the results are listed in Tables 3 and 4; comparisons with the 6-31+G* set including s and p diffuse functions made little difference in the calculated energies and frequencies, and the following discussion will refer to the D95* results. For neutral RuCO, the $^3\Sigma^-$, $^3\Delta$, and ^{5}A states were considered analogous to the FeCO system. In FeCO, the quintet state is very close to the $^3\Sigma^-$ ground state with the $^3\Delta$ state much higher in energy. However, the quintet states for RuCO and OsCO are significantly higher in energy than the $^3\Sigma^-$ and $^3\Delta$ states. For RuCO, the ground state was calculated to be $^3\Delta$, with the $^3\Sigma^-$ state lying 10.8 kcal/mol higher, but for OsCO, the $^3\Sigma^-$ state is 11.5 kcal/mol lower than the $^3\Delta$ state. Both MCO^- anions were calculated to have $^2\Delta$ ground states, and both MCO^+ cations were determined to have $^4\Sigma^-$ ground states. A previous calculation also reported the $^4\Sigma^-$ ground state for $RuCO^+$ cation.[28] We note that Fe and Os share the d^6s^2 electron configuration whereas Ru is d^7s^1.

TABLE 1: Infrared Absorptions (cm^{-1}) from Co-deposition of Laser-Ablated Ru Atoms with CO

A. In Excess Neon at 4 K

$^{12}C^{16}O$	$^{13}C^{16}O$	$^{12}C^{18}O$	$^{12}C^{16}O+^{13}C^{16}O$	R (12/13)	R (16/18)	assignment
2194.3	2145.9			1.0226		CO^+
2140.8	2093.6	2089.7		1.0225	1.0245	CO
2134.9	2087.0	2085.7	2134.9, 2087.0	1.0230	1.0236	$RuCO^+$
2075.3	2026.2	2031.3		1.0242	1.0217	?
2056.3	2010.9	2007.4	2067.4, 2056.4, 2018.4, 2010.9	1.0226	1.0244	$(CO)_2^+$
2051.3	2005.7	2003.5		1.0227	1.0239	$Ru(CO)_5$ site
2049.8	2004.2	2001.8		1.0228	1.0240	$Ru(CO)_5$
2023.5	1979.4	1975.1		1.0223	1.0245	$(Ru_2(CO)_8)$
2018.5	1969.8	1977.0		1.0247	1.0210	?
2012.3	1967.2	1965.8		1.0229	1.0237	$Ru(CO)_5$
1983.0	1938.8	1936.5		1.0228	1.0240	$Ru(CO)_4$
1975.4	1931.8	1928.7	1975.4, 1952.1, 1942.8, 1931.6	1.0226	1.0242	$Ru(CO)_3$
1970.6	1924.8	1927.5	1971.5, 1970.6, 1925.8, 1924.9	1.0238	1.0224	$Ru(CO)_3$
1958.1	1916.0	1910.3		1.0220	1.0250	$Ru(CO)_2$ site
1956.6	1914.6	1908.8	1956.6, 1932.8, 1914.5	1.0219	1.0250	$Ru(CO)_2$ site
1955.3	1913.2	1907.5	1955.3, 1929.9, 1913.2	1.0220	1.0251	$Ru(CO)_2$
1936.5	1890.5	1895.9	1936.6, 1890.6	1.0243	1.0214	RuCO site
1935.6	1889.6	1894.9	1935.6, 1889.6	1.0243	1.0215	RuCO
1929.7	1884.7	1887.9	1929.7, 1901.2, 1884.6	1.0239	1.0221	$Ru_2(CO)_2$
1928.5	1883.6	1886.8	1928.5, 1900.0, 1883.5	1.0238	1.0221	$Ru_2(CO)_2$ site
1907.3	1862.3	1866.8		1.0242	1.0217	Ru_xCO
1881.0	1837.2	1839.4		1.0238	1.0226	$Ru(CO)_4^-$ C_{3v}
1868.6	1826.3	1826.4		1.0232	1.0231	$Ru(CO)_4^-$ C_{3v}
1864.8	1821.6	1823.9		1.0237	1.0224	$Ru(CO)_4^-$ D_{2d}
1862.1	1820.2	1819.5		1.0230	1.0234	$Ru(CO)_4^-$ D_{2d}
1860.1	1818.4	1817.4		1.0229	1.0235	$Ru(CO)_4^-$ D_{2d}
1833.9	1791.2	1794.3		1.0238	1.0221	$Ru(CO)_3^-$ site
1832.9	1790.2	1792.8		1.0239	1.0224	$Ru(CO)_3^-$
1830.6	1787.3			1.0242		$Ru(CO)_2^-$
1823.6	1782.2	1782.4		1.0232	1.0231	$Ru(CO)_3^-$
1822.7	1781.2	1781.5	1822.7, 1809.7, 1787.3, 1781.2	1.0233	1.0231	$Ru(CO)_3^-$ site
1794.2	1752.5	1755.0	1794.1, 1752.5	1.0238	1.0223	Ru_xCO
1792.8	1748.2	1758.4	1792.8, 1748.2	1.0255	1.0196	$RuCO^-$
1769.6	1729.2	1730.3	1769.7, 1744.3, 1743.2, 1729.2	1.0234	1.0227	$Ru(CO)_2^-$ site
1766.5	1726.2	1727.4	1766.5, 1740.6, 1726.2	1.0233	1.0226	$Ru(CO)_2^-$
1517.4	1484.2	1481.2	1517.4, 1499.4, 1484.2	1.0224	1.0244	$(CO)_2^-$
1516.3	1483.0	1490.4	1516.3, 1498.1, 1483.0	1.0225	1.0243	$(CO)_2^-$ site
592.6	527.6	591.8		1.02597	1.00135	$Ru(CO)_5$

B. In Excess Argon at 10 K

$^{12}C^{16}O$	$^{13}C^{16}O$	$^{12}C^{18}O$	$^{12}C^{16}O+^{13}C^{16}O$	$^{12}C^{16}O+^{12}C^{18}O$	R(12/13)	R(16/18)	assignment
2043.1	1997.4	1994.9			1.0229	1.0242	$Ru(CO)_5$ site
2041.5	1996.2	1993.6			1.0227	1.0240	$Ru(CO)_5$ site
2039.1	1993.8	1991.4			1.0227	1.0240	$Ru(CO)_5$
2012.2	1966.9	1965.9			1.0230	1.0236	$(Ru_2(CO)_8)$
2007.6	1962.6	1961.2			1.0230	1.0237	$Ru(CO)_5$ site
2005.5	1960.5	1959.1			1.0230	1.0237	$Ru(CO)_5$ site
2003.8	1958.9	1957.5			1.0229	1.0237	$Ru(CO)_5$
1923.3	1877.8	1882.9	1923.3, 1877.8		1.0242	1.0215	RuCO site
1917.7	1872.3	1877.4	1917.6, 1872.3	1917.6, 1877.3	1.0243	1.0215	RuCO
1915.3	1870.7	1873.7	1915.3, 1889.2, 1870.7	1915.2, 1892.0, 1873.7	1.0238	1.0222	$Ru(CO)_2$
1912.5	1867.9	1871.0			1.0239	1.0222	$Ru(CO)_2$ site
1882.0	1837.3	1842.6			1.0243	1.0214	$Ru(CO)_4^-$ C_{3v}
1862.4	1820.2	1820.2	1862.3, 1820.3	1862.4, 1820.2	1.0232	1.0232	$Ru(CO)_4^-$ C_{3v}
1857	1815				1.023		$Ru(CO)_4^-$ D_{2d}
1834.2	1790.0	1796.8	1834.2, 1817.5, 1790.0	1834.2, 1816.5, 1797.0	1.0247	1.0208	$Ru(CO)_2^-$
1818.2	1776.1	1778.6			1.0237	1.0223	Ru_xCO
1810.3	1768.9	1769.8	1810.3, 1796.0, 1780.0, 1768.9	1810.3, 1797.2, 1780.2, 1769.9	1.0234	1.0229	$Ru(CO)_3^-$
1782.5	1738.2	1748.4	1782.5, 1738.1	1782.5, 1748.5	1.0255	1.0195	$RuCO^-$
1778.1	1733.7	1744.1	1777.9, 1733.7	1777.9, 1743.9	1.0256	1.0195	$RuCO^-$ site
1774.9	1730.7	1741.0	1774.9, 1730.7	1774.9, 1740.9	1.0255	1.0195	$RuCO^-$ site
1773.0	1728.8	1739.4	1773.0, 1728.8	1773.0, 1739.4	1.0256	1.0193	$RuCO^-$ site
1756.9	1715.5	1719.7	1756.9, 1730.6, 1715.5	1756.9, 1734.3, 1719.8	1.0241	1.0216	$Ru(CO)_2^-$
1515.5	1482.2	1479.5	1515.5, 1497.4, 1482.2	1515.5, 1497.4	1.02247	1.02433	$(CO)_2^-$
601.6	583.9	598.1			1.0303	1.0059	$Ru(CO)_5$ site
596.1	578.2	592.6			1.0310	1.0059	$Ru(CO)_5$ site
592.3	574.7	590.1	592.4, 584.2, 575.9		1.0306	1.0037	$Ru(CO)_5$
532.0	517.6	529.8			1.0278	1.0042	$Ru(CO)_4$

Similar calculations were also done for dicarbonyl species, the relative energies, structures are listed in Table 5, and the isotopic C−O stretching frequencies and intensities are listed in Table 6. Analogous to the Fe $(CO)_2$ system, the present

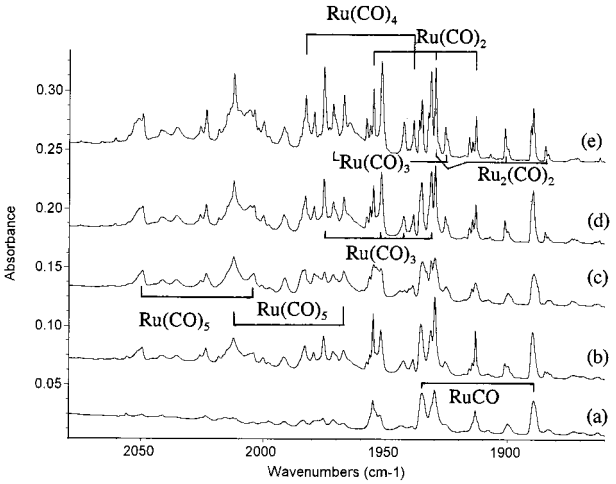

Figure 3. Infrared spectra in the 2080−1880 cm^{-1} region for laser-ablated Ru atoms co-deposited with 0.1% $^{12}C^{16}O$+0.1% $^{13}C^{16}O$ in neon. (a) after 45 min sample deposition at 4 K, (b) after annealing to 8 K, (c) after 10 min full-arc photolysis; (d) after annealing to 10 K; and (e) after annealing to 12 K.

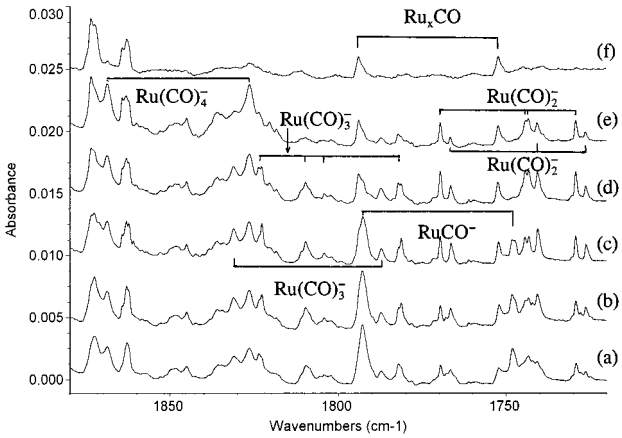

Figure 4. Infrared spectra in the 1880−1720 cm^{-1} region for laser-ablated Ru atoms co-deposited with 0.1% $^{12}C^{16}O$+0.1% $^{13}C^{16}O$ in neon: (a) after 45 min sample deposition at 4 K; (b) after annealing to 6 K; (c) after annealing to 8 K; (d) after 10 min $\lambda > 380$ nm photolysis; (e) after 10 min $\lambda > 290$ nm photolysis; and (f) after 10 min full-arc photolysis.

calculations on $Ru(CO)_2$ and $Os(CO)_2$ also converged to bent and linear structures for the triplet molecules, which are very close in energy. The linear $^3\Delta_g$ state is about 3.0 kcal/mol higher than the bent $^3B_1$ state for $Ru(CO)_2$ using the BP86 functional, but the B3LYP functional predicted the linear state to be 2.2 kcal/mol lower. For $Os(CO)_2$, the linear $^3\Sigma_g^-$ state is 3.6 and 10.4 kcal/mol more stable than the bent $^3B_1$ state using BP86 and B3LYP, respectively. Generally, the linear structure has longer M−C and shorter C−O bonds, and higher C−O stretching vibrational frequencies. Similar situations were also found for dicarbonyl anions. As listed in Table 5, bent and linear structures converged with the linear structures slightly higher in energy. For dicarbonyl cations, only linear structures were considered, both $Ru(CO)_2^+$ and $Os(CO)_2^+$ were calculated to have $^4\Sigma_g^-$ ground states.

The calculation results for tricarbonyls and their anions are listed in Table 7. Both $Ru(CO)_3$ and $Os(CO)_3$ were calculated to have singlet ground states with distorted T-shaped geometries, whereas the triplet with C_{3v} symmetry are 10−12 kcal/mol higher in energy. The nonplanar C_s structure is slightly lower in energy than the planar C_{2v} structure. Similar results were also obtained for the doublet anions.

Finally, calculations were done for tetracarbonyls and their anions, and the results are listed in Table 8. The tetracarbonyls have been studied theoretically by several groups,[18−22] who predicted singlet ground states with C_{2v} symmetry. However, both $Ru(CO)_4$ and $Os(CO)_4$ were converged to D_{2d} symmetry at this level of theory. For anions, two structures were converged, namely C_{3v} and D_{2d}, which are very close in energy with the D_{2d} form slightly lower.

Discussion

Infrared absorptions will be assigned to ruthenium and osmium carbonyl neutral, anion and cation species based on annealing and photolysis behavior, isotopic substitution and DFT isotopic frequency calculations. These experiments were done with low laser energy where metal concentration is less than CO concentration, and the major deposition products are monometal carbonyl species as confirmed by DFT frequency calculations. In addition, the spectrum for the rhodium system (Figure 1) shows weak bands at 2023.5 and 1929.7 cm^{-1} that increase markedly on annealing and are ascribed to dimetal species (Table 1A).

$Ru(CO)_x$ ($x = 1-5$). The prominent 1935.6 cm^{-1} absorption observed on deposition in neon increased on annealing but decreased on photolysis. This band shifted to 1889.6 cm^{-1} in $^{13}C^{16}O$ and 1894.9 cm^{-1} in $^{12}C^{18}O$ experiments giving the 12/13 and 16/18 ratios 1.0243 and 1.0215, respectively. The *increased* 12/13 and *decreased* 16/18 isotopic ratios relative to CO itself indicate that carbon is vibrating between O and a heavy atom.[12,26,27] In the mixed $^{12}C^{16}O$+$^{13}C^{16}O$ experiment, only pure isotopic counterparts were observed, which is appropriate for the RuCO molecule. Our DFT calculation predicted a 1933.5 cm^{-1} C−O stretching vibration for the $^3\Delta$ ground-state RuCO molecule and the 12/13 and 16/18 ratios 1.0252 and 1.0210, which are in excellent agreement with the observed ratios. The scale factor, observed/calculated, 1.0010, is in accord with other pure density functional calculations for transition metal compounds and the LANL basis set.[28]

There is growth of RuCO on annealing in solid neon, so reaction 1 proceeds readily despite the spin change. The identification of $^3\Delta$ as the ground state will have to rest on the

$$Ru(^5F) + CO(^1\Sigma^+) \rightarrow RuCO(^3\Delta) \qquad (1)$$

calculated relative energy below the $^3\Sigma^-$ state as the 12/13 and 16/18 isotopic ratios are the same for both states. The prominent 1917.7 cm^{-1} argon matrix band exhibits the *same* isotopic ratios and is assigned to $^3\Delta$ RuCO in solid argon. The 19.7 cm^{-1} blue shift on going from the solid argon to neon medium shows that there is matrix interaction with RuCO because this state has a 3.8 D calculated dipole moment.

The 1955.3 cm^{-1} absorption observed on deposition in neon increased on annealing. In lower CO concentration experiments, this band was weak after deposition, but increased more on annealing than the RuCO absorption. In the mixed $^{12}C^{16}O$+$^{13}C^{16}O$ experiment, a clear triplet with 1/2/1 relative intensities was observed, which confirms that two equivalent CO submolecules are involved in this vibration, and this band is assigned to the antisymmetric C−O vibration of the $Ru(CO)_2$ molecule. The lack of a symmetric C−O stretching vibration suggests that this molecule has linear or near-linear geometry. Note that the isotopic ratios 12/13 (1.0220) and 16/18 (1.0251) are considerably different from the RuCO values. Present DFT calculation predicted that linear and bent $Ru(CO)_2$ are very close in energy; the $^3\Delta_g$ state is 3.0 kcal/mol higher and 2.2 kcal/mol lower in

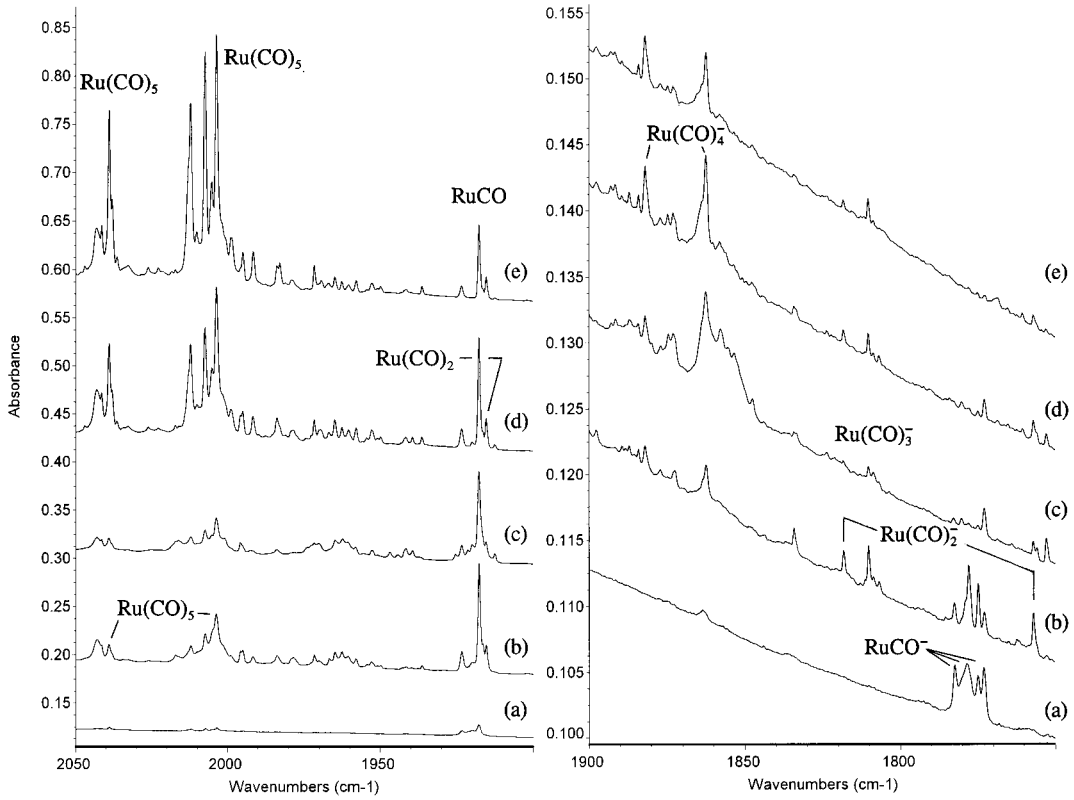

Figure 5. Infrared spectra in the 2050−1900 and 1900−1750 cm^{-1} regions for laser-ablated Ru atoms co-deposited with 0.2% CO in argon: (a) after 60 min sample deposition at 10 K; (b) after annealing to 25 K; (c) after 10 min full-arc photolysis; (d) after annealing to 30 K; and (e) after annealing to 35 K.

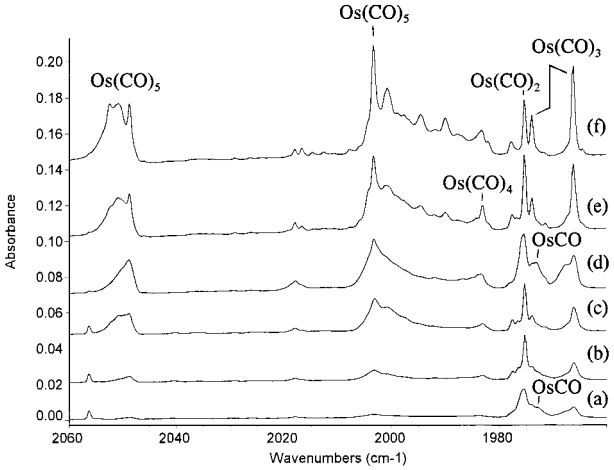

Figure 6. Infrared spectra in the 2060−1960 cm^{-1} region for laser-ablated Os atoms co-deposited with 0.2% CO in neon. (a) after 30 min sample deposition at 4 K; (b) after annealing to 6 K; (c) after annealing to 8 K; (d) after 10 min full-arc photolysis; (e) after annealing to 10 K; and (f) after annealing to 12 K.

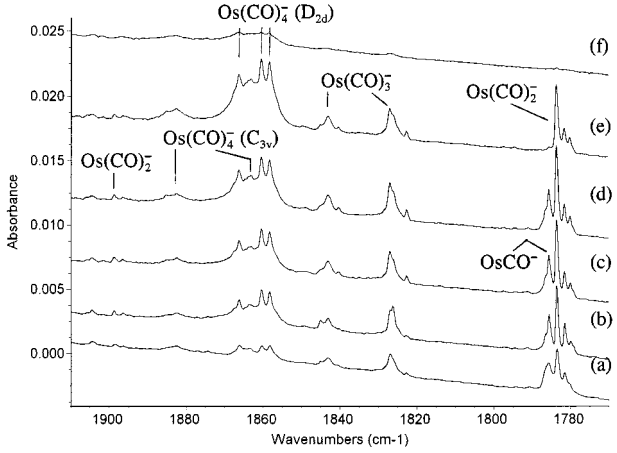

Figure 7. Infrared spectra in the 1910−1770 cm^{-1} region for laser-ablated Os atoms co-deposited with 0.2% CO in neon: (a) after 30 min sample deposition at 4 K; (b) after annealing to 8 K; (c) after 10 min $\lambda > 470$ nm photolysis; (d) after 10 min $\lambda > 380$ nm photolysis; (e) after 10 min $\lambda > 290$ nm photolysis; and (f) after 10 min full-arc photolysis.

energy than $^3B_1$ state with BP86 and B3LYP calculations, respectively. Note the calculated frequency and isotopic frequency ratios (1.0230 and 1.0244) for the linear structure are in excellent agreement with observed experimental values (scale factor, 1.0043), which indicates that the $Ru(CO)_2$ molecule is linear and has a C−O stretching normal mode different from RuCO. In contrast, the argon matrix experiment reveals that the 1915.3 cm^{-1} band increases on annealing and falls *below* the 1917.7 cm^{-1} RuCO absorption. This band is probably due to $Ru(CO)_2$ with the bent structure ($^3B_2$ state) in solid argon. Notice that the difference between calculated antisymmetric C−O stretching modes for linear ($^3\Delta_g$) and bent ($^3B_2$) $Ru(CO)_2$ is 35 cm^{-1}, and the difference between neon and argon matrix $Ru(CO)_2$ bands is 40 cm^{-1}. A similar structural change was found for $Fe(CO)_2$ on going from solid neon to argon as the more polarizable medium can stabilize the bent, polar molecule. The 1929.7 cm^{-1} band that appears on later annealing is also due to a dicarbonyl, most likely the dimer of RuCO.

The 1975.4 and 1970.6 cm^{-1} absorptions increased together on annealing next to the $Ru(CO)_2$ absorption. These bands shifted to 1931.8, 1924.8 cm^{-1} and 1928.7, 1927.5 cm^{-1} in $^{13}C^{16}O$ and $^{12}C^{18}O$ spectra, respectively. The isotopic 12/13 ratio for the lower band (1.0238) is higher than the upper band (1.0226), whereas the 16/18 ratio for the lower band (1.0224) is lower than the upper band (1.0242), which shows that these

TABLE 2: Infrared Absorptions (cm^{-1}) from Co-deposition of Laser-Ablated Os Atoms with CO in Excess Neon at 4 K

$^{12}C^{16}O$	$^{13}C^{16}O$	$^{12}C^{18}O$	$^{12}C^{16}O+^{12}C^{16}O$	R (12/13)	R (16/18)	assignment
2124.3	2077.7	2073.6		1.0224	1.0245	$(Os(CO)_2^+)$
2106.0	2056.9	2060.2		1.0239	1.0222	$OsCO^+$
2052.4	2006.3	2005.0		1.0230	1.0236	$Os(CO)_5$ site
2050.8	2004.7	2003.5		1.0230	1.0236	$Os(CO)_5$ site
2048.7	2002.8	2001.3		1.0229	1.0237	$Os(CO)_5$
2018.0	1970.7	1974.4		1.0240	1.0221	?
2003.4	1957.8	1958.0		1.0233	1.0232	$Os(CO)_5$
2000.8	1955.6	1955.4		1.0231	1.0232	$Os(CO)_5$ site
1989.9	1945.8	1943.8		1.0227	1.0237	?
1983.1	1938.5	1937.5		1.0230	1.0235	$Os(CO)_4$
1977.6	1934.4	1930.4	1977.6, 1951.4, 1934.3	1.0223	1.0245	$Os(CO)_2$ site
1975.2	1931.9	1928.0	1975.2, 1949.1, 1932.0	1.0224	1.0245	$Os(CO)_2$
1973.8	1926.9	1932.4	1973.8, 1972.4, 1926.9, 1925.6	1.0243	1.0214	$Os(CO)_3$
1972.6	1925.2		1972.5, 1925.3	1.0246		OsCO
1966.2	1922.1	1920.8	1966.1, 1945.9, 1934.8, 1922.1	1.0229	1.0236	$Os(CO)_3$
1898.8	1851.8	1861.7	1898.8, 1879.3, 1851.9	1.0254	1.0199	$Os(CO)_2^-$
1896.5	1849.6	1859.3	1896.5, 1877.2, 1849.6	1.0254	1.0200	$Os(CO)_2^-$ site
1882.6	1838.2	1842.7		1.0242	1.0217	$Os(CO)_4^-$ C_{3v}
1866.3	1822.0	1827.2		1.0243	1.0214	$Os(CO)_4^-$ D_{2d}
1862 br	1819	1821		1.0236	1.0225	$Os(CO)_4^-$ C_{3v}
1860.4	1817.7	1819.1		1.0235	1.0227	$Os(CO)_4^-$ D_{2d}
1858.3	1815.7	1816.9		1.0235	1.0228	$Os(CO)_4^-$ D_{2d}
1845.0	1800.7	1806.9		1.0246	1.0211	$Os(CO)_3^-$ site
1843.1	1799.2	1805.2	1840.1, 1797.4	1.0244	1.0210	$Os(CO)_3^-$
1840.4	1796.3	1802.2		1.0246	1.0212	$Os(CO)_3^-$ site
1826.9	1784.8	1786.8	1826.9, 1793.2, 1784.7	1.0236	1.0224	$Os(CO)_3^-$
1826.2	1784.1	1786.0		1.0236	1.0225	$Os(CO)_3^-$ site
1822.6	1780.5	1782.6		1.0236	1.0224	$Os(CO)_3^-$ site
1785.5	1740.9	1753.8	1785.5, 1740.8	1.0256	1.0181	$OsCO^-$
1783.5	1742.8	1743.6	1783.5, 1759.0, 1742.8	1.0234	1.0229	$Os(CO)_2^-$
1781.5	1740.9	1741.6	1781.5, 1757.1, 1740.9	1.0233	1.0229	$Os(CO)_2^-$ site
1780.0	1739.4	1740.1	1780.1, 1755.6, 1739.4	1.0233	1.0229	$Os(CO)_2^-$

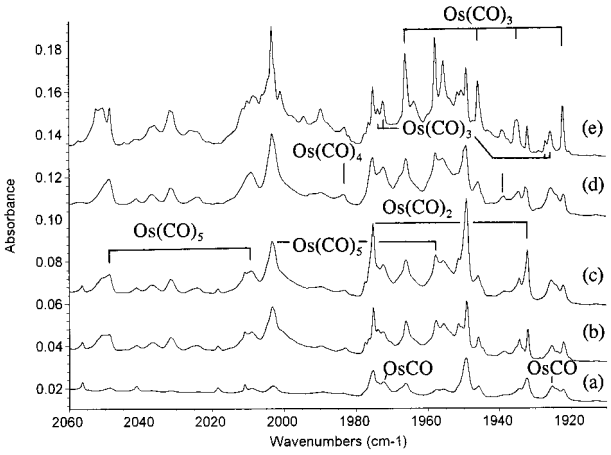

Figure 8. Infrared spectra in the 2060−1910 cm^{-1} region for laser-ablated Os atoms co-deposited with 0.1% $^{12}C^{16}O$+0.1% $^{13}C^{16}O$ in neon: (a) after 45 min sample deposition at 4 K; (b) after annealing to 8 K; (c) after 10 min $\lambda > 380$ nm photolysis; (d) after 10 min full-arc photolysis; and (e) after annealing to 10 K.

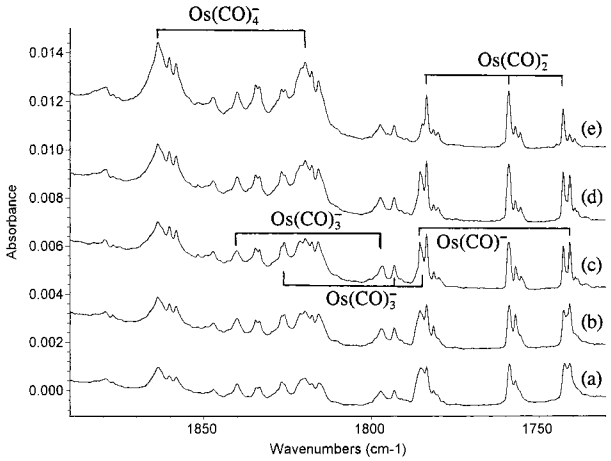

Figure 9. Infrared spectra in the 1890−1730 cm^{-1} region for laser-ablated Os atoms co-deposited with 0.1% $^{12}C^{16}O$+0.1% $^{13}C^{16}O$ in neon: (a) after 45 min sample deposition at 4 K; (b) after annealing to 6 K; (c) after annealing to 8 K; (d) after 10 min $\lambda > 380$ nm photolysis; and (e) after 10 min $\lambda > 290$ nm photolysis.

modes have different C and O movements. In mixed $^{12}C^{16}O+^{13}C^{16}O$ spectra, a quartet with intermediates at 1952.1 and 1942.8 cm^{-1} was observed for the stronger upper band, the sum of two intermediates is about twice as strong as the pure isotopic counterparts, which indicates that this vibrational mode involves *two equivalent* CO subunits *perturbed by another inequivalent* CO. For the lower band, four obvious bands were observed in the mixed spectra, the pure isotopic counterparts, which are weaker, and two bands at 1971.5 and 1925.9 cm^{-1}, which are about two times stronger than pure isotopic counterparts. These two bands are assigned to the axial and equatorial C−O stretching vibrations of the T-shaped $Ru(CO)_3$ molecule. DFT calculation predicted the nonplanar $Ru(CO)_3$ structure slightly lower in energy; however, the calculated isotopic frequencies and intensities for the C_{2v} structure fit experimental values much better, which suggests that $Ru(CO)_3$ has the planar C_{2v} geometry. The scale factors for these modes, 1.0015 and 1.0012, are almost identical and in the range expected for this level of theory. Of more importance, the different 12/13 and 16/18 ratios calculated for each mode (Table 7) *match the unique observed values* for these two modes extremely well. Finally, in the gas phase transient infrared spectrum, a broad 1988 cm^{-1} band has been assigned to the $Ru(CO)_3$ molecule formed by photolysis of $Ru(CO)_5$,[24] which is in agreement with the neon matrix bands allowing for matrix shift.

The 1983.0 cm^{-1} band that grows on annealing is assigned to the $Ru(CO)_4$ molecule, which has been observed near 1998

TABLE 3: States, Relative Energies, Dipole Moments, and Geometries Calculated (BP86/D95*/ECP) for RuCO, $RuCO^-$, $RuCO^+$, OsCO, $OsCO^-$ and $OsCO^+$

molecule	state	energies[a]	dipole[b]	bond lengths (Å); angles (°)
RuCO	$^3\Delta$ ($\sigma^1\delta^3\pi^4$)	0.0	3.8	1.802, 1.190; 180
	$^3\Sigma^-$ ($\sigma^2\delta^2\pi^4$)	+10.8	3.3	1.816, 1.182; 180
	^{5}A ($\sigma^1\sigma^1\delta^2\pi^4$)	+40.3	0.9	1.975, 1.182; 150.3
$RuCO^-$	$^2\Delta$ ($\sigma^2\delta^3\pi^4$)	−28.5	1.7	1.757, 1.217; 180
	$^4\Delta$ ($\sigma^1\sigma^1\delta^3\pi^4$)	−12.8	1.9	1.843, 1.211; 180
$RuCO^+$	$^4\Sigma^-$ ($\sigma^1\delta^2\pi^4$)	+190.0	2.8	1.899, 1.157; 180
OsCO	$^3\Sigma^-$ ($\sigma^2\delta^2\pi^4$)	0.0	2.9	1.785, 1.189; 180
	$^3\Delta$ ($\sigma^1\delta^3\pi^4$)	+11.5	3.7	1.790, 1.195; 180
	^{5}A ($\sigma^1\sigma^1\delta^2\pi^4$)	+38.0	0.7	1.914, 1.185; 164.7
$OsCO^-$	$^2\Delta$ ($\sigma^2\delta^3\pi^4$)	−33.3	2.8	1.764, 1.226; 180
	$^4\Sigma^-$ ($\sigma^1\delta^2\pi^4$)	−21.9	0.2	1.828, 1.212; 180
$OsCO^+$	$^4\Sigma^-$ ($\sigma^1\delta^2\pi^4$)	+197.1	2.1	1.835, 1.164; 180
RuCO	($^3\Delta$)[c]	0.0	4.0	1.804, 1.186; 180
	($^3\Sigma^-$)[c]	+10.9	3.5	1.189, 1.178; 180
$RuCO^-$	($^2\Delta$)[c]	−31.1	2.2	1.757, 1.214; 180
$RuCO^+$	($^4\Sigma^-$)[c]	+190.6	2.9	1.906, 1.152; 180
OsCO	($^3\Sigma^-$)[c]	0.0	3.1	1.787, 1.185; 180
	($^3\Delta$)[c]	+11.5	3.9	1.792, 1.192; 180
$OsCO^-$	($^2\Delta$)[c]	−36.5	3.2	1.763, 1.222; 180
$OsCO^+$	($^4\Sigma^-$)[c]	+197.3	2.2	1.843, 1.160; 180

[a] kcal/mol. [b] Calculated dipole moments in Debye units. [c] The 6-31+G* basis set for C and O.

TABLE 4: Isotopic Frequencies (cm^{-1}), Intensities (km/mol), and Isotopic Frequency Ratios Calculated (BP86/D95*/ECP) for the Monocarbonyl Structures Described in Table 3

molecule	$^{12}C^{16}O$	$^{13}C^{16}O$	$^{12}C^{18}O$	R (12/13)	R (16/18)
RuCO ($^3\Delta$)	1933.5 (518)	1885.9 (492)	1893.8 (498)	1.0252	1.0210
	570.3 (0.4)	563.9 (0.4)	553.1 (0.2)	1.0113	1.0311
	370.9 (8)	359.6 (7)	366.5 (9)	1.0314	1.0120
($^3\Sigma^-$)	1979.9 (545)	1931.2 (517)	1939.2 (526)	1.0252	1.0210
	563.5 (1)	557.1 (1)	546.5 (1)	1.0115	1.0311
	352.4 (12)	341.7 (11)	348.2 (12)	1.0313	1.0121
(^{5}A)	1896.0 (901)	1853.2 (856)	1851.2 (865)	1.0231	1.0242
	451.6 (12)	440.5 (10)	445.4 (13)	1.0252	1.0139
	255.8 (40)	251.1 (39)	249.0 (38)	1.0187	1.0273
$RuCO^-$ ($^2\Delta$)	1811.7 (1043)	1764.7 (991)	1778.1 (1004)	1.0266	1.0189
	621.8 (1)	615.6 (1)	601.8 (1)	1.0101	1.0332
	396.6 (6)	384.5 (5)	392.0 (6)	1.0315	1.0117
$RuCO^+$ ($^4\Sigma^-$)	2102.7 (294)	2053.5 (276)	2055.6 (288)	1.0240	1.0229
	466.3 (6)	460.5 (6)	453.1 (5)	1.0126	1.0291
	336.8 (1)	326.7 (1)	332.7 (1)	1.0309	1.0123
OsCO ($^3\Sigma^-$)	1976.9 (640)	1925.9 (603)	1939.8 (622)	1.0265	1.0192
	634.7 (6)	627.3 (6)	612.6 (4)	1.0118	1.0361
	436.2 (2)	422.9 (2)	430.9 (2)	1.0314	1.0123
($^3\Delta$)	1940.9 (609)	1890.8 (575)	1904.5 (591)	1.0265	1.0191
	630.0 (2)	622.6 (3)	608.0 (2)	1.0119	1.0362
	423.5 (3)	410.6 (3)	418.4 (4)	1.0314	1.0122
(^{5}A)	1922.5 (489)	1877.0 (606)	1880.2 (610)	1.0242	1.0225
	491.4 (5)	483.2 (4)	477.9 (6)	1.0170	1.0282
	207.5 (62)	201.9 (58)	204.0 (59)	1.0277	1.0172
$OsCO^-$ ($^2\Delta$)	1808.8 (997)	1760.0 (944)	1778.2 (964)	1.0277	1.0172
	648.0 (0.6)	641.3 (0.9)	624.2 (0.3)	1.0104	1.0381
	433.1 (0.3)	419.8 (0.2)	428.0 (0.4)	1.0317	1.0119
$OsCO^+$ ($^4\Sigma^-$)	2094.2 (385)	2042.5 (360)	2051.3 (379)	1.0253	1.0209
	584.0 (14)	576.5 (14)	564.6 (12)	1.0130	1.0344
	409.1 (0.4)	396.7 (0.4)	404.1 (0.4)	1.0312	1.0124
RuCO ($^3\Delta$)[a]	1926.3 (547)	1879.3 (519)	1886.2 (526)	1.0250	1.0212
RuCO ($^3\Sigma^-$)[a]	1975.6 (570)	1927.3 (544)	1934.3 (555)	1.0251	1.0213
$RuCO^-$ ($^2\Delta$)[a]	1791.6 (1248)	1745.6 (1185)	1757.9 (1201)	1.0264	1.0192
$RuCO^+$ ($^3\Sigma^-$)[a]	2106.8 (287)	2057.8 (269)	2059.1 (281)	1.0238	1.0232
OsCO ($^3\Sigma^-$)[a]	1966.9 (661)	1916.6 (623)	1929.3 (643)	1.0262	1.0195
$OsCO^-$ ($^2\Delta$)[a]	1788.7 (1191)	1740.9 (1127)	1757.8 (1151)	1.0275	1.0176
$OsCO^+$ ($^4\Sigma^-$)[a]	2090.2 (374)	2039.2 (349)	2046.4 (369)	1.0250	1.0214

[a] The 6-31+G* basis set on C and O.

cm^{-1} in the gas phase[24] and at 1972, 1955 cm^{-1} in solid methane.[23] This band also exhibited carbonyl C−O stretching vibrational ratios [12/13 (1.0228), 16/18 (1.0240)], and no obvious intermediates were observed in the mixed experiment. Our DFT calculation predicted a strong doubly degenerate C−O stretching vibration (e mode) at 1978.5 cm^{-1} (scale factor, 1.0022) with isotopic frequency ratios in very good agreement with values for the $Ru(CO)_4$ molecule with D_{2d} symmetry. Calculation also predicted the a_1 mode at 1997.4 cm^{-1} with much lower intensity, which is not observed here.

The weak 2012.3 and 2049.8 cm^{-1} absorptions that increased markedly on higher temperature annealing in solid neon are

TABLE 5: Geometries and Relative Energies (kcal/mol) Calculated for $M(CO)_2$, $M(CO)_2^-$, and $M(CO)_2^+$

	molecule	state	relative energy	geometry M−C (Å), C−O (Å), ∠CMC (°), ∠MCO (°)
BP86	$Ru(CO)_2$	$^3\Delta_g$	+3.0	1.955, 1.172; 180.0, 180.0
		$^3B_2$	0.0	1.877, 1.181; 102.1, 169.4
	$Ru(CO)_2^-$	$^2\Delta_g$	−35.2	1.920, 1.192; 180.0, 180.0
		$^2A_1$	−42.2	1.872, 1.208; 127.0, 164.2
		$^2B_2$	−42.2	1.822, 1.207; 99.7, 168.7
	$Ru(CO)_2^+$	$^4\Sigma_g^-$	+195.6	2.021, 1.150; 180.0, 180.0
	$Os(CO)_2$	$^3\Sigma_g^-$	0.0	1.930, 1.171; 180.0, 180.0
		$^3B_2$	+3.6	1.857, 1.186; 107.7, 170.6
	$Os(CO)_2^-$	$^2\Delta_g$	−41.3	1.910, 1.197; 180.0, 180.0
		$^2B_1$	−47.6	1.882, 1.205; 144.4, 166.3
		$^2B_2$	−48.9	1.820, 1.211; 102.6, 170.2
	$Os(CO)_2^+$	$^4\Sigma_g^-$	+195.5	1.975, 1.154; 180.0, 180.0
B3LYP	$Ru(CO)_2$	$^3\Delta_g$	0.0	1.971, 1.157; 180.0, 180.0
		$^3B_2$	+2.2	1.904, 1.165; 102.8, 170.4
	$Ru(CO)_2^-$	$^2\Delta_g$	−31.0	1.924, 1.178; 180.0, 180.0
		$^2A_1$	−33.4	1.886, 1.191; 132.0, 166.6
		$^2B_2$	−30.2	1.829, 1.192; 99.7, 169.1
	$Os(CO)_2$	$^3\Sigma_g^-$	0.0	1.937, 1.157; 180.0, 180.0
		$^3B_2$	+10.4	1.868, 1.170; 108.3, 171.3
	$Os(CO)_2^-$	$^2\Delta_g$	−32.5	1.911, 1.182; 180.0, 180.0
		$^2B_1$	−37.3	1.887, 1.190; 146.3, 167.5
		$^2B_2$	−35.1	1.822, 1.197; 102.3, 170.5

TABLE 6: Calculated (BP86) Isotopic C−O Stretching Vibrational Frequencies (cm^{-1}), Intensities (km/mol), and Isotopic Frequency Ratios for the Dicarbonyl Structures Described in Table 5

molecule	$(12-16)_2$	$(13-16)_2$	$(12-18)_2$	R (12/13)	R (16/18)
$Ru(CO)_2$	2043.7 (0) (σ_g)	1994.5 (0)	1999.9 (0)	1.0247	1.0219
($^3\Delta_g$)	1947.0 (2026) (σ_u)	1903.3 (1907)	1900.6 (1972)	1.0230	1.0244
($^3B_2$)	1966.2 (339) (a_1)	1919.3 (322)	1923.4 (326)	1.0244	1.0223
	1911.6 (1218) (b_2)	1867.1 (1145)	1868.5 (1188)	1.0238	1.0231
$Ru(CO)_2^-$	1938.1 (0) (σ_g)	1889.9 (0)	1898.6 (0)	1.0255	1.0208
($^2\Delta_g$)	1826.2 (2650) (σ_u)	1784.1 (2500)	1784.2 (2572)	1.0236	1.0235
($^2A_1$)	1833.7 (425) (a_1)	1788.4 (406)	1796.2 (404)	1.0253	1.0209
	1775.1 (1882) (b_2)	1732.9 (1780)	1736.3 (1820)	1.0244	1.0223
($^2B_2$)	1841.2 (764) (a_1)	1795.2 (729)	1804.3 (730)	1.0256	1.0205
	1782.6 (1208) (b_2)	1739.2 (1140)	1745.2 (1173)	1.0250	1.0214
$Ru(CO)_2^+$	2162.4 (0) (σ_g)	2111.7 (0)	2114.0 (0)	1.0240	1.0229
($^4\Sigma_g^-$)	2107.4 (865) (σ_u)	2060.2 (811)	2057.0 (848)	1.0229	1.0245
$Os(CO)_2$	2069.8 (0) (σ_g)	2018.5 (0)	2027.4 (0)	1.0254	1.0209
($^3\Sigma_g^-$)	1967.4 (1983) (σ_u)	1922.4 (1864)	1921.8 (1935)	1.0234	1.0237
($^3B_2$)	1966.6 (343) (a_1)	1917.8 (324)	1926.6 (331)	1.0254	1.0208
	1908.3 (1327) (b_2)	1862.5 (1247)	1867.3 (1295)	1.0246	1.0220
$Os(CO)_2^-$	1934.8 (0) (σ_g)	1885.4 (0)	1897.4 (0)	1.0262	1.0197
($^2\Delta_g$)	1815.5 (2580) (σ_u)	1772.9 (2440)	1774.9 (2495)	1.0240	1.0229
($^2B_1$)	1887.4 (210) (a_1)	1839.2 (200)	1851.1 (201)	1.0262	1.0196
	1789.5 (2057) (b_2)	1746.9 (1948)	1750.5 (1987)	1.0244	1.0223
($^2B_2$)	1849.9 (740) (a_1)	1802.1 (702)	1815.3 (711)	1.0265	1.0191
	1791.6 (1329) (b_2)	1746.5 (1255)	1756.4 (1289)	1.0258	1.0200
$Os(CO)_2^+$	2157.6 (0) (σ_g)	2105.7 (0)	2111.3 (0)	1.0246	1.0219
($^4\Sigma_g^-$)	2084.2 (1093) (σ_u)	2037.1 (1022)	2034.8 (1073)	1.0231	1.0243

assigned to the $Ru(CO)_5$ molecule with D_{3h} symmetry according to previous gas phase and matrix work.[13,14,24] Strong argon matrix counterparts were observed for $Ru(CO)_5$ at 2003.8 and 2039.1 cm^{-1}, which explains the absence of $Ru(CO)_{3,4}$ because these singlet species rapidly combine with CO to form $Ru(CO)_5$.

$Ru(CO)_x^-$ ($x = 1-4$). New bands in the 1900−1750 cm^{-1} region are photosensitive. These bands share the common behavior of reduction to <10% of the former yield on CCl_4 doping. Analogous to the Fe, Co, Ni, and Cu systems, anion species must be considered.[12,26−28,38]

The 1792.8 cm^{-1} band decreased on annealing and disappeared on $\lambda > 380$ nm photolysis. The $^{13}C^{16}O$ and $^{12}C^{18}O$ counterparts at 1748.2 and 1758.4 cm^{-1} gave isotopic ratios [12/13 (1.0255), 16/18 (1.0196)], which are characteristic of C−O stretching modes where C is bonded to a heavy metal center and vibrating *between* the M and O atoms. In the mixed $^{12}C^{16}O+^{13}C^{16}O$ experiment, only pure isotopic counterparts were presented, which indicates that only one CO subunit is involved. This band is assigned to the $RuCO^-$ anion. Our DFT calculation predicted the $^2\Delta$ ground-state $RuCO^-$ anion to have a C−O stretching vibration at 1811.7 cm^{-1} with the calculated ratios [12/13 (1.0266), 16/18 (1.0189)] in excellent agreement with observed values. This agreement both in frequency position (scale factor, 0.990) and *unique isotopic frequency ratios* confirms the $RuCO^-$ assignment. Strong argon matrix counterparts for $RuCO^-$ were observed at 1782.5 to 1773.0 cm^{-1}, site split much the same as $FeCO^-$ in solid argon.[12]

Sharp bands at 1766.5 and 1769.6 cm^{-1} increased on annealing and $\lambda > 380$ nm photolysis when the $RuCO^-$ and $(CO)_2^-$ absorptions disappeared, then decreased on $\lambda > 290$ nm photolysis, and disappeared on full-arc photolysis. In the mixed $^{12}C^{16}O+^{13}C^{16}O$ spectra, a triplet with 1/2/1 relative intensities was observed for the 1766.5 cm^{-1} band, which is appropriate for the antisymmetric C−O stretching vibration of the $Ru(CO)_2^-$ anion. The 1769.6 cm^{-1} band produced a quartet with two intermediate components separated by 1.1 cm^{-1} in

TABLE 7: Calculated (BP86) Relative Energies (kcal/mol), C−O Isotopic Vibrational Frequencies (cm^{-1}) and Intensities (km/mol) for the Ru and Os Tricarbonyl Molecules and Anions

molecule	energy	$(^{12}C^{16}O)_3$	$(^{13}C^{16}O)_3$	$(^{12}C^{18}O)_3$	R (12/13)	R (16/18)
$Ru(CO)_3$	0	1951.7 (1481)	1907.1 (1398)	1906.3 (1437)	1.0234	1.0238
(^1A)[a]		1962.8 (631)	1915.7 (598)	1920.5 (608)	1.0246	1.0220
		2042.9 (137)	1992.8 (127)	2000.4 (137)	1.0251	1.0212
($^1A_1$)[b]	+2.7	1968.2 (569)	1920.4 (540)	1926.7 (549)	1.0249	1.0215
		1972.0 (1804)	1927.7 (1698)	1925.1 (1757)	1.0230	1.0244
		2071.1 (22)	2020.7 (19)	2027.5 (24)	1.0249	1.0215
$Ru(CO)_3^-$	−46.1	1814.4 (1798)	1771.8 (1705)	1773.9 (1732)	1.0240	1.0228
(^2A) [c]		1830.2 (954)	1786.1 (904)	1791.1 (921)	1.0247	1.0218
		1896.6 (338)	1850.2 (323)	1857.0 (322)	1.0251	1.0213
($^2A_1$)[d]	−42.0	1834.8 (2278)	1792.6 (2160)	1792.5 (2197)	1.0235	1.0236
		1854.8 (1843)	1809.4 (800)	1816.2 (810)	1.0251	1.0213
		1923.2 (98)	1876.0 (91)	1883.3 (97)	1.0252	1.0212
$Os(CO)_3$	0	1948.9 (1512)	1903.5 (1426)	1904.9 (1469)	1.0239	1.0231
(^1A)[e]		1969.1 (699)	1920.5 (662)	1928.8 (674)	1.0253	1.0209
		2042.8 (171)	1991.6 (157)	2002.1 (172)	1.0257	1.0203
($^1A_1$) [f]	+3.4	1973.0 (1846)	1928.1 (1736)	1926.9 (1800)	1.0233	1.0239
		1976.9 (744)	1927.3 (702)	1937.5 (722)	1.0257	1.0203
		2077.1 (27)	2025.6 (23)	2034.8 (30)	1.0254	1.0208
$Os(CO)_3^-$	−52.4	1821.4 (1789)	1777.7 (1698)	1782.2 (1722)	1.0246	1.0220
(^2A)[g]		1845.1 (1006)	1799.2 (952)	1808.0 (970)	1.0255	1.0205
		1909.6 (279)	1861.4 (266)	1872.0 (266)	1.0259	1.0201
($^2A_1$)[h]	−48.6	1836.3 (2187)	1793.2 (2073)	1795.3 (2108)	1.0240	1.0228
		1859.6 (1059)	1812.9 (1004)	1822.7 (1022)	1.0258	1.0202
		1933.2 (42)	1884.4 (38)	1895.1 (43)	1.0259	1.0201

[a] Structure: C_s symmetry, Ru−C (ax): 1.818 Å, C−O: 1.177 Å, ∠RuCO: 178.3°, Ru−C (eq): 1.930 Å, C−O: 1.174 Å, ∠RuCO: 171.6°, $\angle C_{ax}RuC_{eq}$: 89.9°, $\angle C_{eq}RuC_{eq}$: 145.0°. [b] Structure: C_{2v} symmetry, Ru−C (ax): 1.814 Å, C−O: 1.180 Å, Ru−C (eq): 1.953 Å, C−O: 1.168 Å, $\angle C_{ax}RuC_{eq}$: 88.7°. [c] Structure: C_s symmetry, Ru−C (ax): 1.856 Å, C−O: 1.196 Å, ∠RuCO: 175.3°, Ru−C (eq): 1.907 Å, C−O: 1.199 Å, ∠RuCO: 163.9°, $\angle C_{ax}RuC_{eq}$: 98.0°,$\angle C_{eq}RuC_{eq}$: 132.1°. [d]Structure: C_{2v} symmetry, Ru−C (ax): 1.834 Å, C−O: 1.198 Å, Ru−C (eq): 1.938 Å, C−O: 1.192 Å, $\angle C_{ax}RuC_{eq}$: 97.3°. [e] Structure: C_s symmetry, Os−C (ax): 1.823 Å, C−O: 1.181 Å, ∠OsCO: 178.3°, Os−C (eq): 1.921 Å, C−O: 1.177 Å, ∠OsCO: 172.5°, $\angle C_{ax}OsC_{eq}$: 91.5°, $\angle C_{eq}OsC_{eq}$: 145.0°. [f] Structure: C_{2v} symmetry, Os−C (ax): 1.818 Å, C−O: 1.183 Å, Os−C (eq): 1.947 Å, C−O: 1.170 Å, $\angle C_{ax}OsC_{eq}$: 90.2°. [g] Structure: C_s symmetry, Os−C (ax): 1.853 Å, C−O: 1.200 Å, ∠OsCO: 177.0°, Os−C (eq): 1.899 Å, C−O: 1.201 Å, ∠OsCO: 172.3°, $\angle C_{ax}OsC_{eq}$: 99.4°, $\angle C_{eq}OsC_{eq}$: 137.1°. [h] Structure: C_{2v} symmetry, Os−C (ax): 1.840 Å, C−O: 1.201 Å, Os−C (eq): 1.925 Å, C−O: 1.195 Å, $\angle C_{ax}OsC_{eq}$: 100.0°.

TABLE 8: Calculated (BP86) Relative Energies (kcal/mol), C−O Isotopic Vibrational Frequencies (cm^{-1}) and Intensities (km/mol) for Ru and Os Tetracarbonyl Molecules and Anions

molecule	relative energy	$(^{12}C^{16}O)_4$	$(^{13}C^{16}O)_4$	$(^{12}C^{18}O)_4$	R (12/13)	R (16/18)
$Ru(CO)_4$	0	1978.5 (1450) (e)	1933.4 (1367)	1932.3 (1409)	1.0233	1.0239
($^1A_1$)[a]		1978.5 (1450) (e)	1933.4 (1367)	1932.3 (1409)	1.0233	1.0239
		1997.4 (404) (a_1)	1950.2 (382)	1953.5 (391)	1.0242	1.0225
		2076.8 (0) (a_1)	2026.5 (0)	2032.7 (0)	1.0248	1.0217
$Ru(CO)_4^-$	−45.4	1852.4 (1418) (e)	1809.1 (1350)	1810.9 (1359)	1.0239	1.0229
($^2A_1$)[b]		1852.4 (1418) (e)	1809.1 (1350)	1810.9 (1359)	1.0239	1.0229
		1870.9 (768) (a_1)	1826.1 (731)	1830.4 (756)	1.0245	1.0221
		1937.6 (113) (a_1)	1890.8 (107)	1896.3 (109)	1.0248	1.0218
$Ru(CO)_4^-$	−46.9	1850.6 (1664) (e)	1807.5 (1581)	1808.7 (1600)	1.0238	1.0232
($^2B_2$)[c]		1850.6 (1664) (e)	1807.5 (1581)	1808.7 (1600)	1.0238	1.0232
		1857.5 (809) (b_2)	1813.0 (768)	1817.4 (780)	1.0245	1.0221
		1940.2 (0) (a_1)	1893.1 (0)	1899.2 (0)	1.0249	1.0216
$Os(CO)_4$	0	1975.1 (1443) (e)	1929.3 (1360)	1930.2 (1403)	1.0237	1.0233
($^1A_1$)[d]		1975.1 (1443) (e)	1929.3 (1360)	1930.2 (1403)	1.0237	1.0233
		1994.7 (518) (a_1)	1946.5 (488)	1952.3 (502)	1.0248	1.0217
		2075.4 (0) (a_1)	2024.1 (0)	2032.8 (0)	1.0253	1.0210
$Os(CO)_4^-$	−50.9	1855.4 (1379) (e)	1810.8 (1313)	1815.5 (1322)	1.0246	1.0220
($^2A_1$)[e]		1855.4 (1379) (e)	1810.8 (1313)	1815.5 (1322)	1.0246	1.0220
		1878.5 (848) (a_1)	1832.4 (806)	1839.7 (814)	1.0252	1.0211
		1946.3 (123) (a_1)	1897.9 (119)	1907.0 (119)	1.0255	1.0206
$Os(CO)_4^-$	−52.8	1856.3 (1622) (e)	1811.9 (1540)	1816.0 (1560)	1.0245	1.0222
($^2B_2$)[f]		1856.3 (1622) (e)	1811.9 (1540)	1816.0 (1560)	1.0245	1.0222
		1866.8 (881) (b_2)	1820.8 (836)	1828.3 (849)	1.0253	1.0211
		1950.2 (0) (a_1)	1901.4 (0)	1911.1 (0)	1.0257	1.0205

[a] Structure: D_{2d} symmetry, Ru−C: 1.937 Å, C−O: 1.169 Å, ∠CRuC: 149.0°, ∠RuCO: 169.6°. [b] Structure: C_{3v} symmetry, Ru−C (ax): 1.875 Å, C−O: 1.190 Å, ∠RuCO: 180°, Ru−C (eq): 1.941 Å, C−O: 1.191 Å, $\angle C_{eq}RuC_{eq}$: 118.2°, ∠RuCO: 173.2°. $\angle C_{eq}RuC_{ax}$: 97.8°. [c] Structure: D_{2d} symmetry, Ru−C: 1.921 Å, C−O: 1.191 Å, ∠CRuC: 132.8°, ∠RuCO: 175.9°. [d] Structure: D_{2d} symmetry, Os−C: 1.930 Å, C−O: 1.173 Å, ∠COsC: 145.6°, ∠OsCO: 168.5°. [e] Structure: C_{3v} symmetry, Os−C (ax): 1.877 Å, C−O: 1.192 Å, ∠OsCO: 180°, Os−C (eq): 1.923 Å, C−O: 1.194 Å, $\angle C_{eq}OsC_{eq}$: 117.6°, ∠RuCO: 178.9°. $\angle C_{eq}OsC_{ax}$: 99.0°. [f] Structure: D_{2d} symmetry, Os−C: 1.911 Å, C−O: 1.194 Å, ∠COsC: 131.3°, pOsCO: 174.5°.

the mixed spectra, which is probably due to perturbed or slightly distorted $Ru(CO)_2^-$ anion. A weaker band at 1830.6 cm^{-1} tracks with the 1769.6 cm^{-1} band (Figure 2) and shows a larger carbon isotopic ratio, which is due to the symmetric C−O vibration of

the $Ru(CO)_2^-$ anion. Both BP86 and B3LYP calculations predicted the linear structure to be higher in energy and to have an imaginary bending frequency. The bent $^2A_1$ and $^2B_2$ states are almost degenerate using the BP86 functional, whereas B3LYP calculations predicted the $^2A_1$ state to be 3.1 kcal/mol lower. Note that calculated (BP86) C−O stretching vibrational frequencies for the $^2A_1$ state (1775.1 and 1833.7 cm^{-1}) are in excellent agreement with observed values (scale factors, 0.998 and 0.997) and that the unique isotopic ratios (Table 1A) are also fit well by the calculations. Argon matrix counterparts for bent $Ru(CO)_2^-$ were observed at 1756.9 and 1834.2 cm^{-1}, red shifted by 12.7 cm^{-1}, and blue shifted by 3.6 cm^{-1}, respectively.

The 1822.7 and 1832.9 cm^{-1} bands increased together slightly on annealing and $\lambda > 380$ nm photolysis, but were almost eliminated on $\lambda > 290$ nm photolysis. These bands shifted to 1781.2, 1790.2 cm^{-1} in $^{13}C^{16}O$ and 1781.5, 1792.8 cm^{-1} in $^{12}C^{18}O$ experiments, respectively, and the lower band exhibits less 12/13 and more 16/18 ratios than the upper band. In the mixed isotopic experiment, the upper band gave a broad doublet at 1831.1 and 1787.3 cm^{-1}, which actually is an unresolved sextet, the lower band gave two intermediate components at 1809.7 and 1804.3 cm^{-1}, with the 1809.7 cm^{-1} band much stronger than the 1804.3 cm^{-1} band. The mixed isotopic spectra are quite similar to spectra of the $Ru(CO)_3$ molecule. These two bands are assigned to the axial and equatorial C−O stretching vibrations of the T-shaped $Ru(CO)_3^-$ anion. The stronger band was observed at 1810.3 cm^{-1} in solid argon. DFT calculation predicted that $Ru(CO)_3^-$ is also distorted like the neutral $Ru(CO)_3$ molecule. The axial and equatorial C−O stretching vibrations were predicted at 1830.2 and 1814.4 cm^{-1} for the nonplanar ^2A ground-state $Ru(CO)_3^-$ with C_s symmetry. The scale factors (1.001 and 1.005) are near values found here for other Ru carbonyl species.

Broad bands at 1868.6 and 1881.0 cm^{-1} and a weak sharp band set at 1860.1, 1862.1, and 1864.8 cm^{-1} increased on annealing, but only the broad bands increased on photolysis using the $\lambda > 290$ nm filter when the $Ru(CO)_2^-$ and $Ru(CO)_3^-$ anion absorptions markedly decreased, so the next anion $Ru(CO)_4^-$ must be considered. Both C_{3v} and D_{2d} structures were converged in the present DFT calculations for $Ru(CO)_4^-$ with the D_{2d} form slightly lower in energy. As listed in Table 8, our BP86 calculation predicted that the C_{3v} form has a strong doubly degenerate antisymmetric equatorial C−O stretching vibration (e mode) at 1852.4 cm^{-1} and a weaker symmetric axial C−O stretching vibration (a_1 mode) at 1870.9 cm^{-1}, whereas the D_{2d} form has strong doubly degenerate antisymmetric C−O stretching vibration (e mode) at 1850.6 cm^{-1} and a weaker symmetric C−O stretching vibration (b_2 mode) at 1857.5 cm^{-1}. Sharper argon matrix bands were observed at 1862.4 and 1882.0 cm^{-1} for the C_{3v} form, and an 1857 cm^{-1} photolysis product (Figure 5) is probably due to the D_{2d} structure. The calculations strongly suggest assignment of the broad band set at 1868.6 and 1881.0 cm^{-1} to the C_{3v} form and the 1860.1, 1862.1, and 1864.8 cm^{-1} band set to the D_{2d} structure. The degenerate (e) mode of the D_{2d} structure is split into two bands at 1860.1 and 1862.1 cm^{-1} which have the same isotopic ratios, and the weaker 1864.8 cm^{-1} band, which has different isotopic ratios, is assigned to the b_2 mode. Note that the observed isotopic ratios and relative band positions (scale factors, 1.004−1.009) *and intensities* are in very good agreement with calculated values (Table 8). As will be discussed, very similar band sets were observed in the Os+CO system, which further supports these assignments.

$Os(CO)_x$ ($x = 1-5$). The OsCO assignment is not as clear as that for RuCO. Our DFT calculation predicted a $^3\Sigma^-$ ground state with a strong C−O stretching vibration at 1976.9 cm^{-1}. The weak band at 1972.6 cm^{-1} decreased on annealing but increased on broadband photolysis. This band shifted to 1925.2 cm^{-1} using the $^{13}C^{16}O$ reagent, but the $^{12}C^{18}O$ counterpart was covered by strong absorption at 1928.0 cm^{-1}, which will be assigned to the $Os(C^{18}O)_2$ molecule. This weak band is appropriate for the OsCO molecule.

The 1975.2 cm^{-1} band is the major product absorption after deposition, it increased on lower temperature annealing, but decreased on higher temperature annealing. In the mixed $^{12}C^{16}O+^{13}C^{16}O$ experiment, a triplet at 1975.2, 1949.1, and 1932.0 cm^{-1} with 1/2/1 relative intensities was produced. This band is assigned to the antisymmetric C−O stretching vibration of the linear $Os(CO)_2$ molecule, because no symmetric mode candidate was observed to track with this band and DFT calculation predicted a linear $^3\Sigma_g^-$ ground state for the $Os(CO)_2$ molecule. The calculated 1967.4 cm^{-1} C−O stretching vibration frequency is in excellent agreement with the observed 1975.2 cm^{-1} value (scale factor, 1.004).

The sharp absorptions at 1966.2 and 1973.8 cm^{-1} were observed after deposition in higher CO concentration experiments, but in the lowest CO concentration (0.05%) experiment, these bands were observed only after annealing. The lower band intensity is about twice that of the upper band. These two bands increased together on annealing (Figure 6) and shifted to 1926.9, 1922.1 cm^{-1} and 1932.4, 1920.8 cm^{-1} in $^{13}C^{16}O$ and $^{12}C^{18}O$ spectra, respectively. The isotopic 12/13 ratio for the upper band (1.0243) is higher than for the lower band (1.0229), whereas the 16/18 ratio for the upper band (1.0214) is lower than for the lower band (1.0236), which signifies different vibrational modes. In the mixed $^{12}C^{16}O+^{13}C^{16}O$ spectra, a quartet with intermediates at 1945.9 and 1934.8 cm^{-1} was observed for the lower band, whereas the upper band mainly gave four bands at 1973.8, 1972.4, 1926.9, and 1925.6 cm^{-1}. These two bands are assigned to the axial and equatorial C−O stretching vibrations of a distorted T-shaped $Os(CO)_3$ molecule. Note that the mixed isotopic structures are slightly different from that of the $Ru(CO)_3$ molecule. In the former case the equatorial C−O stretching vibration is higher than the axial C−O stretching vibration, hence, in the mixed isotopic spectra, the mixed isotopic counterparts were higher than the pure isotopic counterparts for the axial C−O stretching vibration. Our DFT calculations predicted the antisymmetric axial and equatorial C−O stretching vibrations at 1948.9 and 1969.1 cm^{-1} with (1512:699) intensity ratio for the nonplanar C_s symmetry $Os(CO)_3$ molecule. The planar C_{2v} molecule is slightly higher in energy at this level of theory with two vibrational modes at 1973.0 and 1976.9 cm^{-1} and 1846:744 intensity ratio. The planar results are closer to the observed values (scale factors, 0.997 and 0.998) and suggest that the $Os(CO)_3$ molecule has planar or near planar structure. A broad 1980 cm^{-1} band has been assigned to $Os(CO)_3$ in the gas phase, but the two modes were not resolved.[25]

A weak band was produced at 1983.1 cm^{-1} on annealing after $Os(CO)_3$ but before $Os(CO)_5$ absorptions. This suggests assignment to the antisymmetric C−O stretching vibration of the $Os(CO)_4$ molecule with D_{2d} symmetry, which was observed at about 2000 cm^{-1} in the gas phase[25] and calculated here at 1975.1 cm^{-1}. The symmetric stretching vibration was calculated at 1994.7 cm^{-1} with much weaker intensity and could not be observed here.

The broad bands at 2003.4 and 2048.7 cm^{-1}, which markedly increased to sharp peaks on higher temperature annealing, are assigned to the equatorial C−O stretching (e mode) and axial

C−O stretching (a_2 mode) vibrations of the $Os(CO)_5$ molecule with D_{3h} symmetry. These bands were observed at 2015 and 2045 cm^{-1} in the gas phase.[25]

$Os(CO)_x^-$ ($x = 1-4$). All the absorptions in the 1900−1770-cm^{-1} region are photosensitive and almost eliminated by CCl_4 doping, so anion species must be considered analogous to the Fe and Ru systems. The 1785.5 cm^{-1} band slightly sharpened on annealing and disappeared on photolysis using $\lambda > 290$ nm. This band shifted to 1740.9 cm^{-1} in $^{13}C^{16}O$ and to 1753.8 cm^{-1} in $^{12}C^{18}O$ spectra, and gave large 12/13 (1.0256) and small 16/18 (1.0181) ratios. In the mixed $^{12}C^{16}O+^{13}C^{16}O$ spectra, only pure isotopic absorptions were presented, so only one CO submolecule is involved, which is appropriate for the $OsCO^-$ anion. The C−O stretching vibration of the ground state ($^2\Delta$) $OsCO^-$ anion was calculated at 1808.8 cm^{-1} with isotopic ratios [12/13 (1.0277), 16/18 (1.0172)]. The frequency position is in very good agreement (scale factor, 0.987) with the observed values, as are the extreme isotopic ratios, although the carbon participation is overestimated, which supports the anion assignment.

A sharp 1783.5 cm^{-1} band increased on annealing to 6 and 8 K and on $\lambda > 380$ nm photolysis when the $(CO)_2^-$ absorption decreased. This band slightly decreased (−30%) on $\lambda > 290$ nm photolysis and disappeared on full-arc photolysis. In the mixed $^{12}C^{16}O+^{13}C^{16}O$ experiment, a triplet with approximately 1/2/1 relative intensities was produced. This band is assigned to the antisymmetric C−O vibration of the $Os(CO)_2^-$ anion. A weaker sharp 1898.8 cm^{-1} band has the same annealing and photolysis behaviors and shows a larger 12/13 ratio and a lower 16/18 ratio. This band is assigned to the symmetric C−O stretching vibration of the $Os(CO)_2^-$ anion. As listed in Table 6, our BP86 calculation predicted the two stretching vibrations for the most stable bent $Os(CO)_2^-$ anion ($^2B_1$) at 1789.5 and 1887.4 cm^{-1} with 10:1 relative intensities. Again, note the excellent match among calculated frequency positions, isotopic ratios, and observed values.

The 1826.9 and 1843.1 cm^{-1} bands increased together on 6 and 8 K annealing and on $\lambda > 380$ nm photolysis, slightly decreased on $\lambda > 290$ nm photolysis, and disappeared on full-arc photolysis. These two bands are assigned to the equatorial and axial C−O stretching vibrations of the $Os(CO)_3^-$ anion following $Ru(CO)_3^-$. As listed in Table 7, DFT calculation predicted 1821.4 and 1845.1 cm^{-1} axial and equatorial C−O stretching vibrations for the nonplanar $Os(CO)_3^-$ anion. The planar C_{2v} structure has slightly higher energy, and gave 1836.3 and 1859.6 cm^{-1} vibrational frequencies. Because both sets of calculated frequencies and isotopic ratios fit the observations very well, it is not possible to determine the structure from our calculations.

Broad bands at 1862, 1882.6 cm^{-1} and sharp bands at 1858.3, 1860.4, and 1866.3 cm^{-1} increased on annealing and $\lambda > 290$ nm photolysis when the other anion absorptions decreased or disappeared. These two band sets have almost the same behavior as the band sets in the Ru+CO system, which were assigned to $Ru(CO)_4^-$ anions with C_{3v} and D_{2d} symmetry. As listed in Table 8, calculation predicted that the C_{3v} form has strong doubly degenerate antisymmetric equatorial C−O stretching vibration (e mode) at 1855.4 cm^{-1} and symmetric axial C−O stretching vibration (a_1 mode) at 1878.5 cm^{-1}, whereas the D_{2d} form has strong doubly degenerate antisymmetric C−O stretching vibration (e mode) at 1856.3 cm^{-1} and symmetric C−O stretching vibration (b_2 mode) at 1856.8 cm^{-1}. The calculated frequencies strongly support assignment of the broad bands to C_{3v} $Os(CO)_4^-$ and the sharp bands to D_{2d} $Os(CO)_4^-$. Again, the degenerate mode of the D_{2d} structure is split into two bands at 1858.3 and 1860.4 cm^{-1}, which have the same intensities and isotopic ratios. Note the observed isotopic ratios and relative band positions and intensities are in very good agreement with calculated values for both structures (scale factors, 1.002−1.005).

Both calculations and experiments suggest that the $Fe(CO)_3^-$ anion has D_{3h} symmetry.[2,30] In contrast, the present work shows that both $Ru(CO)_3^-$ and $Os(CO)_3^-$ are distorted to T-shaped C_{2v} symmetry. The $Fe(CO)_3^-$ anion can combine with another CO to form the $Fe(CO)_4^-$ anion with C_{3v} symmetry, as both calculation and experiments also indicated.[2,30,31] In Ru and Os, the $Ru(CO)_3^-$ and $Os(CO)_3^-$ anions are distorted, so when $Ru(CO)_3^-$ and $Os(CO)_3^-$ combine with another CO molecule the two possibilities are to form D_{2d} or C_{3v} symmetry $Ru(CO)_4^-$ and $Os(CO)_4^-$ anions. Our BP86 calculations predicted the C_{3v} and D_{2d} structures of the $Ru(CO)_4^-$ and $Os(CO)_4^-$ anions to be very close in energy, and both anion structures were observed in the neon matrix. The relative yield of the D_{2d} structure anion increased from Ru to Os, and the D_{2d} form of $Ru(CO)_4^-$ was observed only after photolysis in solid argon.

As discussed in our iron carbonyl investigations, the $M(CO)_x^-$ ($x = 1-3$) anions originate from electron capture by the neutral carbonyls formed on sample deposition as these electron affinities (EA) range from 1.2 to 1.8 eV.[2] Added CCl_4 intercepts ablated electrons and prevents

$$RuCO\ (^3\Delta) + e^- \rightarrow RuCO^-\ (^2\Delta) \qquad (2)$$

the formation of carbonyl anions. On annealing the addition of more CO occurs leading to increasing x values and the formation of the $x = 4$ anion,[12] which has an even higher 2.4-eV electron affinity for the iron species.[2] Photolysis of these samples photodetaches anions, including $(CO)_2^-$, and these electrons reattach to carbonyls with higher electron affinities, and the ultimate electronic trap namely cations. We found for the iron system that the photon energy required for anion destruction increased with x value, as observed in the gas phase,[2] although we need at least 1 eV more photon energy for photolysis in the matrix than in the gas phase.

Because there is no gas phase work on the Ru and Os carbonyl anions, the present experiments provide the only available photodetachment information. The above-mentioned trend of increasing photon energy to destroy higher carbonyl anions also holds for Ru and Os. In neon matrix experiments, the $RuCO^-$ anion is destroyed under photolysis conditions ($\lambda > 380$ nm) that *do not* affect $FeCO^-$ and $OsCO^-$; hence, the EA of RuCO (a $^3\Delta$ state) is probably less than FeCO ($^3\Sigma^-$) (measured 1.2 eV in gas phase[2]) but the EA of OsCO is probably comparable with FeCO. On the other hand, $Ru(CO)_2^-$ and $Os(CO)_2^-$ are more robust than $Fe(CO)_2^-$ to this visible light. The dicarbonyls of Ru and Os may have higher EAs than $Fe(CO)_2$ (experimental, 1.2 eV in gas phase[2]). We note that $\lambda > 290$ nm photolysis slightly increases $Fe(CO)_3^-$, but $Ru(CO)_3^-$ is almost destroyed, and $Os(CO)_3^-$ is decreased about 20%. Hence, $Os(CO)_3$ probably has a lower EA than $Fe(CO)_3$ with $Ru(CO)_3$ considerably lower. With 290 nm cutoff photolysis, the stable $Fe(CO)_4^-$ increases markedly (3×) and the isostructural (C_{3v}) Ru and Os tetracarbonyl anions increase (+50%), whereas the D_{2d} isomer increases for Os but not Ru in solid neon (Figures 2 and 7). We conclude that $Ru(CO)_4$ and $Os(CO)_4$ have considerable EAs, perhaps almost as high as $Fe(CO)_4$. This growth on near-UV photolysis is due to electron capture reaction 3 and implies that the small angle change involved in this rearrangement proceeds readily. We suggest that the D_{2d} form, which is probably less stable, arises mostly

from reaction 4, but a small increase in the D_{2d} isomer is observed on visible (blue) photolysis.

$$M(CO)_4\ (D_{2d}) + e^- \rightarrow M(CO)_4^-\ (C_{3v}) \qquad (3)$$

$$M(CO)_3^-\ (C_{2v}, \text{T-shaped}) + CO \rightarrow M(CO)_4^-\ (D_{2d}) \qquad (4)$$

$RuCO^+$, $OsCO^+$. Sharp weak bands at 2134.9 cm^{-1} in Ru+CO and 2106.0 cm^{-1} in Os+CO experiments greatly increased on annealing to 6 and 8 K, and were eliminated by full-arc photolysis, as were all carbonyl anions. These bands were enhanced 3 × relative to the neutral absorptions with CCl_4 doping as is appropriate for cation species.[12] In the mixed $^{12}C^{16}O+^{13}C^{16}O$ isotopic experiment, there is no obvious intermediate isotopic component. These two bands are assigned to the $RuCO^+$ and $OsCO^+$ cations after the $FeCO^+$ cation at 2123.0 cm^{-1}. Our DFT calculations gave 2102.7 cm^{-1} and 2094.2 cm^{-1} C−O stretching frequencies for the $RuCO^+$ and $OsCO^+$ cations, which are in good agreement with observed values (scale factors, 1.015 and 1.006). The $RuCO^+$ cation is formed on deposition from laser-ablated Ru^+ cations, and the reaction of Ru^+ and CO in the cold matrix proceeds on annealing to 6 and 8 K.

$$Ru^+\ (^4F) + CO(^1\Sigma^+) \rightarrow RuCO^+\ (^4\Sigma^-) \qquad (5)$$

Conclusions

In addition to preparing the Ru and Os carbonyls ($x = 1-5$), monocarbonyl cations, and carbonyl anions ($x = 1-4$) for infrared spectroscopic characterization in solid neon from laser-ablated metal atoms, cations, and electrons, this work provides a unique data set for comparison with density functional calculations for frequency and intensity prediction and normal mode description through isotopic shifts. First, BP86/D95*/ECP+DZ calculations predict the frequencies of $Ru(CO)_x$ ($x = 1-4$) with scale factors 1.001 to 1.004, the corresponding anion frequencies with scale factors 0.990 to 1.005, the $RuCO^+$ and $OsCO^+$ cations with scale factors 1.015 and 1.006, the $Os(CO)_x$ ($x = 2-4$) frequencies with 0.997 to 1.004 scale factors, and the $Os(CO)_x^-$ ($x = 1-4$) frequencies (nine values) with 0.987−1.006 scale factors (average value, 1.000). These scale factors compare with values reported for transition metal compounds, using the 6-311G* and LANL2DZ basis sets, and the S−VWN (1.0168) and B-LYP (1.0371) pure density functionals.[38]

Second, the ^{13}CO and $C^{18}O$ isotopic shifts for carbonyl vibrations (generally 42−45 cm^{-1}) are reproduced by these DFT calculations within averages of 1 cm^{-1} for the Ru compounds and 2 cm^{-1} for the Os species reported here. This is not as good as the 0.5−1.0 cm^{-1} average isotopic shift fits found for iron and other first-row transition metal carbonyls.[12,26,27] Note that the isotopic ratios change slightly from MCO to MCO^- to MCO^+ as the normal mode change reflects the M−CO bond lengths and that the isotopic ratios change little with the larger basis set on C and O (Tables 3 and 4).

Third, it is remarkable how well these DFT calculations predict spectra of the C_{2v} T-shaped structures for both $M(CO)_3^-$ anions, and of C_{3v} *and* D_{2d} structures for both $M(CO)_4^-$ anions (Table 8). For the $Os(CO)_4^-$ C_{3v} case, a strong (e) mode at 1855.4 cm^{-1} is predicted with 2 × 1379 km/mol intensity and a weaker (a_1) mode at 1878.5 cm^{-1} with 848 km/mol intensity. The spectrum (Figure 7) shows broad bands at 1862 and 1882.6 cm^{-1} with > 2:1 relative intensity (scale factors, 1.0036 and 1.0022). For the D_{2d} case, the strong (e) mode calculated at 1856.3 cm^{-1} is split by the matrix at 1858.3, 1860.4 cm^{-1}; and the weaker (b_2) mode calculated at 1856.8 cm^{-1} is observed at 1866.3 cm^{-1}. The calculated relative intensity 2 × 1622:881 is matched by experiment within the error of band intensity measurement. Comparable agreement is found for both ruthenium tetracarbonyl anion structures.

TABLE 9: Neon Matrix Frequencies (cm^{-1}) for Fe, Ru, and Os Carbonyl Cations, Molecules, and Anions

carbonyl	Fe	Ru	Os
$M(CO)_2^+$	2134	−	2124
MCO^+	2123	2135	2106
$M(CO)_5$	2035, 2011	2050, 2012	2049, 2003
$M(CO)_4$	2001, 1983	1983	1983
$M(CO)_3$	1945	1975, 1971	1974, 1966
$M(CO)_2$	1917	1955	1975
MCO	1934	1936	1973
$M(CO)_4^-$	1860	1881, 1869[a]	1883, 1862[a]
		1865, 1860[b]	1866, 1860[b]
$M(CO)_3^-$	1795	1833, 1824	1843, 1827
$M(CO)_2^-$	−, 1733	1831, 1767	1899, 1784
MCO^-	1782	1793	1786

[a] C_{3v} structure. [b] D_{2d} structure.

Because the $Ru(CO)_x^-$ and $Os(CO)_x^-$ anions have not been examined by gas-phase photodetachment spectroscopy, the matrix photolysis data relative to the analogous matrix[12] and gas-phase[2] $Fe(CO)_x^-$ studies provides some useful information. Although the EA of OsCO is probably comparable to the EA of FeCO (1.2 eV),[2] the EA of RuCO is somewhat lower. The dicarbonyls of Ru and Os probably have higher EAs than the Fe compound, but the heavier tri- and tetracarbonyls likely have lower EAs than $Fe(CO)_4$. Adding diffuse functions to the basis set (6-31+G*) gives slightly more stable anions and frequencies closer to the observed values.

Some interesting chemical comparisons can be made among the carbonyl cations, molecules, and anions of Fe, Ru, and Os, Table 9. The carbonyl chromophore is a sensor for the electronic environment, and the comparison of MCO^q species ($q = +$, o, $-$) carbonyl frequencies provides some measure of the available electronic charge. The Ru monocarbonyl cation, neutral, and anion frequencies in solid neon are 12, 2, and 11 cm^{-1} higher than the Fe cation, neutral, and anion, respectively, but the Os species are 29 cm^{-1} lower, 37 cm^{-1} higher, and 7 cm^{-1} lower than the Ru species. The OsCO ($^3\Sigma^-$) frequency is higher relative to RuCO ($^3\Delta$) in part because of the state change. Note even closer agreement for the larger carbonyls of Ru and Os. At first it may be surprising that these differences are so small because in coordination complexes these differences are generally larger. For example, the $[M^{II}(NH_3)_5CO]X_2$ (M = Ru, Os; X = Cl, Br) complexes have been examined,[42] and the C−O frequency is 1925 or 1930 cm^{-1} for Ru and 1888 or 1892 cm^{-1} for Os. Two points of comparison are important: the position of these carbonyl frequencies and the Ru → Os shift. First, the position is in the range of neutral RuCO and OsCO values, or slightly lower. This strongly suggests that the $M^{II}(NH_3)_5$ center to which CO is coordinated is nearly neutral and certainly not M^{2+} as formally written. Second, the 37-cm^{-1} red shift from Ru to Os suggests more effective d-π* back-bonding for Os, which is only matched by our $RuCO^+$ and $OsCO^+$ species.

Mulliken charges[32] were calculated for the ruthenium carbonyl species and are given below with carbonyl stretching frequencies.

+0.94 +0.01 +0.05	+0.14 0.0 0.14	−0.85 +0.13 −0.28
$RuCO^+$	RuCO	$RuCO^-$
2135 cm^{-1} (calc)	1934 cm^{-1} (calc)	1812 cm^{-1} (calc)
2103 cm^{-1} (obs)	1936 cm^{-1} (obs)	1793 cm^{-1} (obs)

A similar DFT calculation for the "isolated" $(Ru(NH_3)_5CO)^{2+}$ dication gave a strong 2117 cm^{-1} carbonyl frequency and

Mulliken charges on axial NH_3 (+0.25), equatorial NH_3 (+0.29), Ru (+0.53), C (+0.09), and O (−0.04). It is clear that the metal center is intermediate between that found in our $RuCO^+$ and RuCO species, both in Mulliken charge and in carbonyl frequency, and that the amine ligands effectively delocalize substantial positive charge from the metal cation center. The same calculation for $(Os(NH_3)_5CO)^{2+}$ provided a strong 2090 cm^{-1} carbonyl mode and Mulliken charges on axial NH_3 (+0.26), equatorial NH_3 (+0.31), Os (+0.64), C (−0.07), and O (−0.07) for comparison.

The RuCO frequency observed here in solid neon, 1936 cm^{-1}, may be compared with the 1984 cm^{-1} frequency for CO on Ru(001) at very low coverage.[43,44] The interaction with a single atom in RuCO is clearly stronger than the interaction with the metal surface.

Finally, the linear $Ru(CO)_2$ frequency in solid neon, 1955 cm^{-1}, may be compared with 2064 and 2002 cm^{-1} frequencies for a bent $Ru^I(CO)_2$ species on zeolite.[45] Although we did not observe isolated $Ru(CO)_2^+$, the antisymmetric fundamental of linear $Ru(CO)_2^+$ is predicted at 2160 cm^{-1} from the present DFT calculations. We conclude from the present work that the $Ru^I(CO)_2$ species on zeolite has a local charge near one-half. Similar conclusions have been reached for $Rh^I(CO)_2$ species.[46]

Acknowledgment. We gratefully acknowledge National Science Foundation support for this research under grant CHE 97-00116 and A. Citra for performing the M^{II} complex ion calculations.

References and Notes

(1) Cotton, F. A.; Wilkinson, G. *Advanced Inorganic Chemistry*, 5th ed.; Wiley: New York, 1988.
(2) Engelking, P. C.; Lineberger, W. C. *J. Am. Chem. Soc*. **1979**, *101*, 5569. Villalta, P. W.; Leopold, D. G. *J. Chem. Phys*. **1993**, *98*, 7730.
(3) Schulz, R.; Crellin, K. C.; Armentrout, P. B. *J. Am. Chem. Soc*. **1991**, *113*, 8590.
(4) Ryther, R. J.; Weitz, E. *J. Phys. Chem*. **1991**, *95*, 9841; **1992**, *96*, 2561.
(5) Tanaka, K.; Sakaguchi, K.; Tanaka, T. *J. Chem. Phys.* **1997**, *106*, 2118, and references therein.
(6) Bililign, S.; Feigerle, C. S.; Miller, J. C.; Velegrakis, M. *J. Chem. Phys.* **1998**, *108*, 6312, and references therein.
(7) Barnes, L. B.; Rosi, M.; Bauschlicher, C. W., Jr. *J. Chem. Phys.* **1991**, *94*, 2031.
(8) Ricca, A.; Bauschlicher, C. W., Jr.; Rosi, M. *J. Phys. Chem*. **1994**, *98*, 9498; Ricca, A.; Bauschlicher, C. W., Jr. *Theor. Chim. Acta* **1995**, *92*, 123.
(9) Barnes, L. A.; Rosi, M.; Bauschlicher, C. W., Jr. *J. Chem. Phys.* **1990**, *93*, 609; Ricca, A.; Bauschlicher, C. W., Jr. *J. Phys. Chem.* **1994**, *98*, 12899, and references therein.
(10) Ricca, A.; Bauschlicher, C. W., Jr. *J. Phys. Chem.* **1995**, *99*, 5922, and references therein.
(11) Castro, M.; Salahub, D. R.; Fournier, R. *J. Chem. Phys.* **1994**, *100*, 8233, and references therein.
(12) Zhou, M. F.; Chertihin, C. V.; Andrews, L. *J. Chem. Phys.* **1998**, *109*, 10893; Zhou, M. F.; Andrews, L. *J. Chem. Phys.* **1999**, *110*, 10370.
(13) Calderazzo, F.; L'Eplattenier, F. *Inorg. Chem.* **1967**, *6*, 1220.
(14) Rushman, P.; van Buuren, G. N.; Shiraian, M.; Pomeroy, R. K. *Organometallics* **1983**, *2*, 693.
(15) Gregory, M. F.; Poliakoff, M.; Turner, J. J. *J. Mol. Struct.* **1985**, *127*, 247.
(16) Huang, J.; Hedberg, K.; Davis, H. B.; Pomeroy, R. K. *Inorg. Chem.* **1990**, *29*, 3923.
(17) Huang, J.; Hedberg, K.; Pomeroy, R. K. *Organometallics* **1988**, *7*, 2049.
(18) Ziegler, T.; Tschinke, V.; Ursen, C. *J. Am. Chem. Soc.* **1987**, *109*, 4825.
(19) Delley, B.; Wrinn, M.; Luthi, H. P. *J. Chem. Phys.* **1994**, *100*, 5785.
(20) Ehlers, A. W.; Frenking, G. *Organometallics* **1995**, *14*, 423.
(21) Li, J.; Schreckenbach, G.; Ziegler, T. *J. Am. Chem. Soc.* **1995**, *117*, 486.
(22) Decker, S. A.; Klobukowski, M. *J. Am. Chem. Soc.* **1998**, *120*, 9342.
(23) Poliakoff, M.; Turner, J. J. *J. Chem. Soc., Dalton Trans.* **1974**, 2276.
(24) Bogdan, P. L.; Weitz, E. *J. Am. Chem. Soc.* **1989**, *111*, 3163.
(25) Bogdan, P. L.; Weitz, E. *J. Am. Chem. Soc.* **1990**, *112*, 639.
(26) Zhou, M.; Andrews, L. *J. Phys. Chem.* A **1998**, *102*, 10250.
(27) Zhou, M.; Andrews, L. *J. Am. Chem. Soc.* **1998**, *120*, 11499.
(28) Zhou, M.; Andrews, L. *J. Chem. Phys.* **1999**, *110*, 2414.
(29) Burkholder, T. R.; Andrews, L. *J. Chem. Phys.* **1991**, *95*, 8697.
(30) Hassanzadeh, P.; Andrews, L. *J. Phys. Chem.* **1992**, *96*, 9177.
(31) Thompson, W. E.; Jacox, M. E. *J. Chem. Phys.* **1991**, *95*, 735.
(32) Frisch, M. J.; Trucks, G. W.; Schlegel, H. B.; Gill, P. M. W.; Johnson, B. G.; Robb, M. A.; Cheeseman, J. R.; Keith, T.; Petersson, G. A.; Montgomery, J. A.; Raghavachari, K.; Al-Laham, M. A.; Zakrzewski, V. G.; Ortiz, J. V.; Foresman, J. B.; Cioslowski, J.; Stefanov, B. B.; Nanayakkara, A.; Challacombe, M.; Peng, C. Y.; Ayala, P. Y.; Chen, W.; Wong, M. W.; Andres, J. L.; Replogle, E. S.; Gomperts, R.; Martin, R. L.; Fox, D. J.; Binkley, J. S.; Defrees, D. J.; Baker, J.; Stewart, J. P.; Head-Gordon, M.; Gonzalez, C.; Pople, J. A. *Gaussian 94, Revision B.1* Gaussian, Inc.: Pittsburgh, PA, 1995.
(33) Perdew, J. P. *Phys. Rev. B* **1986**, *33*, 8822. Becke, A. D. *J. Chem. Phys.* **1993**, *98*, 5648.
(34) Lee, C.; Yang, E.; Parr, R. G. *Phys. Rev. B* **1988**, *37*, 785.
(35) Dunning, T. H., Jr.; Hay, P. J. In *Modern Theoretical Chemistry*; Schaefer, H. F., III, Ed.; Plenum: New York, 1976.
(36) Hay, P. J.; Wadt, W. R. *J. Chem. Phys* **1985**, *82*, 299.
(37) Barnes, L. S.; Rosi, M.; Bauschlicher, C. W., Jr. *J. Chem. Phys.* **1990**, *93*, 609.
(38) Bytheway, I.; Wong, M. H. *Chem. Phys. Lett*. **1998**, *282*, 219.
(39) Zhou, M. F.; Andrews, L. *J. Chem. Phys.* **1999**, *110*, in press.
(40) Ricca, A.; Bauschlicher, C. W., Jr. *J. Phys. Chem.* **1995**, *99*, 5922.
(41) Breeze, P. A.; Burdett, J. K.; Turner, J. J. *Inorg. Chem*. **1981**, *20*, 3369.
(42) Bee, M. W.; Kettle, F. A.; Powell, D. B. *Spectrochim. Acta* **1974**, *30A*, 585.
(43) Thompson, G. E.; Weinberg, W. H. *J. Chem. Phys.***1979**, *70*, 1437.
(44) Pfnur, H.; Menzel, D.; Hoffman, F. M.; Ortega, A.; Bradshaw, A. M. *Surf. Sci.* **1980**, *93*, 431.
(45) Conners, L.; Hollis, T.; Johnson, D. A.; Blyholder, G. *J. Phys. Chem. B* **1998**, *102*, 10112.
(46) Zhou, M. F.; Andrews, L. *J. Phys. Chem. A* **1999**, in press.